UNIVERSITÀ DEGLI STUDI DI GENOVA

Scuola di Scienze Mediche e farmaceutiche
Corso di Laurea in Medicina e Chirurgia

PhD Thesis

ROLE OF ADVANCED MRI SEQUENCES IN PREDICTING THE OUTCOME OF PRETERM NEONATES

Ph.D. Course

NEUROSCIENCE

Curriculum

CLINICAL and EXPERIMENTAL NEUROSCIENCES

Cycle

XXXI (2015-2018)

Candidate:

Dr. Domenico Tortora MD

University of Genoa

Tutor: Dr. Andrea Rossi MD

U.O. Neuroradiologia

Istituto G. Gaslini Genova

Coordinator: Prof. Angelo Schenone

University of Genoa

Table of Contents:

1. Abstract.....2

2. Introduction.....4

2.1 Prematurity.....4

2.2 Brain lesions at different stages of prematurity.....4

2.3 Long-term outcome in preterm neonates.....7

2.4 Long-term outcome in preterm neonates with normal brain MRI.....8

2.5 Conventional neonatal MR Imaging and neurodevelopmental outcome 9

2.6 Advanced MRI sequences for neonatal brain study.....10

3. Rationale.....15

4. Results.....16

4.1 Study Population.....16

4.2 First Year Results.....16

4.2.1 Variability of subependymal vein anatomy in neonates as evaluated with MR SWI-venography.....16

4.2.2 Differences in subependymal vein anatomy may predispose preterm infants to GMH–IVH..26

4.3 Second Year Results.....36

4.3.1 The effects of mild germinal matrix-intraventricular haemorrhage on the developmental white matter microstructure of preterm neonates: a DTIs tudy.....36

4.3.2 Prematurity and brain perfusion: Arterial Spin Labeling MRI.....49

4.4 Third Year Results.....62

4.4.1 Quantitative susceptibility map analysis in preterm neonates with germinal matrix-intraventricular hemorrhage 62

5. Conclusions 74

6. Future developments 75

7. References.....76

8. List of publications 79

1. ABSTRACT

AIM

The aim of the project is to evaluate the role of advanced MRI sequences (susceptibility weight imaging (SWI), diffusion tensor imaging (DTI), and arterial spin labeling (ASL) perfusion) in detecting early changes that affect preterm neonatal brain, especially in those patients without lesions at conventional MRI or with small brain injuries (i.e. low grade germinal matrix-intraventricular hemorrhage (GMH-IVH)), and to correlate these subtle brain abnormalities with neurodevelopmental outcome at 24 months.

METHODS

Since November 2015 until June 2017, 287 preterm neonates and 108 term neonates underwent a 3T or 1.5T MRI study at term corrected age (40±1 weeks). SWI, DTI and ASL sequences were performed in all neonates. SWI sequences were evaluated using both a qualitative (SWI venography) and quantitative (Quantitative Susceptibility Map analysis (SWI-QSM)) approach. DTI data were analyzed using a Tract-Based Spatial Statistics analysis (TBSS). ASL studies were processed to estimate Cerebral Blood Flow (CBF) maps. Perinatal clinical data were collected for all neonates. Neurodevelopmental data were evaluated at 24 months in 175 neonates using 0-2 Griffiths Developmental Scales.

RESULTS

The analysis performed on SWI-venography revealed differences in subependymal veins morphology between preterm and term neonates with normal brain MRI, with a higher variability from the typical anatomical pattern in preterm neonates. The same analysis performed in preterm neonates with GMH-IVH revealed that the anatomical features of subependymal veins may play a potential role as predisposing factor for GMH-IVH. Moreover, the SWI-QSM analysis revealed a greater paramagnetic susceptibility in several periventricular white matter (WM) regions in preterm neonates with GMH-IVH than in healthy controls. This finding is likely related to the accumulation of hemosiderin/ferritin following the diffusion of large amounts of intraventricular blood products into the WM, and it is also supposed to trigger the cascade of lipid peroxidation and free radical formation that promote oxidative and inflammatory injury of the WM in neonatal brain after GMH-IVH. The TBSS analysis confirmed that microstructural WM injury can occur in preterm neonates with low grade GMH-IVH even in the absence of overt signal changes on conventional MRI, with different patterns of WM involvement depending on gestational age. Moreover, the distribution of these WM microstructural alterations

after GMH-IVH correlates with specific neurodevelopmental impairments at 24 months of age. Finally, the analysis of brain perfusion at term-corrected age revealed lower CBF in preterms with sub-optimal neuromotor development, reinforcing the hypothesis that impaired autoregulation of CBF may contribute to the development of brain damage in preterm neonates.

CONCLUSION

Advanced MRI sequences can assist the standard perinatal brain imaging in the early diagnosis of preterm neonatal brain lesions and can provide new insights for predicting the neurodevelopmental trajectory. However, detailed and serial imaging of carefully chosen cohorts of neonates coupled with longer clinical follow-up are essential to ensure the clinical significance of these novel findings.

2. INTRODUCTION

2.1 Prematurity

Preterm births account for approximately 12% of live births in Europe[1] and are associated with an increased risk of infant mortality, morbidity, and neurodevelopmental disabilities. Preterm infants were previously at high risk for destructive brain lesions that resulted in cystic white matter injury and secondary cortical and subcortical gray matter degeneration with consequent neurodevelopmental disabilities including cerebral palsy and motor dysfunction.

The recent exponential increase in detailed magnetic resonance imaging studies has placed greater attention on the idea of gestationally determined regional brain vulnerability with the site and nature of the injury sustained being determined by a combination of the characteristics of the insult, the specific tissue and cell vulnerability and the gestational age of the infant.

In order to understand the vulnerability of the immature brain to injury, it is essential to consider the stages of brain development. The first half of gestation is characterized by neuronal proliferation and migration. During the second half, glial cell proliferation and programmed cell death predominate. The last trimester of gestation is characterized by developing connectivity, so axonal and dendritic sprouting and synapse formation are predominant. Regional tissue vulnerability at a given gestational age is likely to be determined by the local metabolic requirements together with specific cell characteristics that increase the vulnerability of such cells to injury.

2.2 Brain lesions at different stages of prematurity

2.2.1 Germinal matrix - intraventricular hemorrhage

The brain of an *extremely preterm* infants (23-26 weeks) is characterized by significant developmental changes that are especially noticeable in the cerebellum and in the periventricular zone, both of which host the germinal matrix. The germinal matrix, that is situated on the surface of the lateral ventricles, increases in volume and reaches its maximum volume at about 25 weeks of gestation after which it decreases dramatically[1].

The germinal and subventricular layers are sites of neuronal and glial cell proliferation and migration and represent also a common site of injury in the preterm brain. It is vulnerable to both hemorrhagic injury, as a result of the dense vascular

network, and to injury from infection, e.g. by cytomegalovirus, which can result in necrosis and cyst formation.

Impaired cerebrovascular autoregulation with frequent fluctuations in carbon oxide, disturbances in coagulation, large patent ductus arteriosus and other parameters compromising the brain circulation, may affect the regions with rich capillary networks. Due to the poor vascular integrity of involuting immature vessels and inadequate connective tissue support with a deficiency in mesenchymal and glial elements, the capillary network is vulnerable to rupture and hemorrhage. From a clinical perspective, even more than respiratory distress syndrome (with its fluctuating pattern of systemic blood pressure, high risk of hypercapnia and pneumothorax), Apgar score at birth, hypotension and genetic thrombophilic patterns are the most consistently recognized predisposing factors to these hemorrhagic lesions in very premature infants[1–3].

Germinal matrix-intraventricular haemorrhage (GMH-IVH) is a major complication of prematurity and one of the main causes of morbidity and mortality[2]. The inverse relationship with gestational age indicates that the larger the matrix, the more susceptible it is to haemorrhage, thus highlighting that these neonates are the most unstable and require the most critical intensive care in the neonatal period.

2.2.2 Periventricular leukomalacia

The vulnerability of the brain in *early preterm* period (26-34 weeks) is mainly connected to the white matter development, especially in the periventricular zones[4]. Genesis of the vulnerability appears to be multifactorial, relating to vessel anatomy with regions of relatively poor perfusion, low baseline blood flow, impaired regulation of blood flow, and the inherent susceptibility of pre-oligodendrocytes to damage[5]. The vasoconstriction of the cerebral vessels that follows hypocarbia, which can occur during high frequency mechanical ventilation, may also play a significant role in the pathogenesis of the injury[6].

In addition, it has been suggested that the presence of numerous resident microglia in the immature brain increases its susceptibility to white matter injury. Both hypoxia-ischemia and infection lead to microglia activation, resulting in free radicals and glutamate release. Immature oligodendrocytes demonstrate specific vulnerability to oxidative stress[7] and glutamate receptor immaturity[8], so the ultimate result would be deficit of mature oligodendroglia, and a consequent impairment of myelination.

Periventricular leukomalacia (PVL) represent the most frequent form of white

matter injury in early preterm neonates[9]. PVL has two neuropathological components: i) a focal periventricular necrotic component with cellular and axonal swelling and astrocytic and microglial proliferation; and ii) a component with diffuse gliosis in the surrounding cerebral white matter. There are two types of necrotic foci with different histopathological/neuroimaging evolutions: macroscopic (necrosis > 1 mm that evolves over several weeks into a cyst, also referred to as "cystic PVL") and microscopic (necrosis ≤ 1 mm that evolves over several weeks into glial scars, also referred to as "punctate lesions")[10]

Imaging studies have emphasized that the most severe forms of PVL could be associated with secondary abnormalities involving the entire thalamo-cortical circuit, giving rise to thalamic atrophy and a decrease in cortical volume[11]. Although the incidence of the most severe cystic forms of PVL is decreasing, multiple punctate lesions, that are predominately linearly organized at the borders of the lateral ventricles, remain among the most frequent lesions in preterm neonatal brain[12]. Caution is needed when interpreting isolated punctuate lesions seen on MRI since their clinical significance with regard to long-term outcome is not yet well defined[13].

2.2.3 Diffuse white matter gliosis

Diffuse white matter gliosis (DWMG) is a rather common neuropathological finding in postmortem studies of early preterm neonates (41%). Nevertheless, the incidence for this pattern in preterm infant survivors is unknown, as well as its impact on long-term neurodevelopmental outcome[13,14]. DWMG has been defined by diffuse astrocytic activation in cerebral white matter and, unlike PVL, it lacks focal necrotic components and the associated neuronal–axonal loss[15,16]. Despite preterm infants usually presents DWMG at term corrected age, several studies demonstrated that this finding has a low predictive value for the neurological long-term outcome at 3 years. Thus, it also suggests that DWMG may represent a mild microstructural WM injury or WM maturational delay or, more likely, both etiologies[14].

2.2.4 Hypoxic-ischemic encephalopathy

The neuromorbidity of *late preterm* infants (34-36 weeks) has been attributed to many factors, since these children remain at risk of injuries that are traditionally associated with more preterm infants as well as of those that are typical of at-term newborns. Vulnerability of specific neuronal populations in the late preterm period is due to multiple factors (i.e. coagulation disorders, hypoglycemia and infections) but, like white matter vulnerability in the early-preterm brain, excitotoxicity and oxidative stress may play a significant role in brain lesions at this stage. In particular, in late preterm neonates the characteristic over-expression of glutamate receptors in

regions like the basal ganglia, necessary for long-term potentiation and connectivity, can lead to the production of nitrogen and oxygen free radicals after an insult, leading to the injury of nearby cells[17]. Basal ganglia and thalami are also recognized as metabolically active zones with increased energy requirements which contribute to their particular vulnerability to acute hypoxic insults[10].

Studies of hypoxic-ischemic encephalopathy (HIE) in late preterm neonates demonstrate that in this category hypoxic insult mainly affects the grey matter, but the sites may differ compared to the more mature term brain. Basal ganglia are most frequently involved, particularly the ventrolateral thalami and posterior putamen, as occurs in term babies. Late preterm infants are more likely to show brainstem lesions compared to term infants[18], indicating an increased susceptibility of the brainstem at these slightly younger gestational ages[19]. Less frequently, injury may also occur to the cerebral cortex and subcortical white matter, which are, on the contrary, more frequently involved in term infants. It is likely that this region becomes more vulnerable at term due to its active myelination during the very last weeks of gestation[18]. This observation confirms that the metabolic demands of myelination may compound the increased vulnerability of cortical neurons and brainstem at different gestational ages, according to the different stages of maturation.

Ischemic lesions of the basal ganglia and thalami are associated with cerebral palsy and cognitive impairment. In the case of a severe insult, these lesions can be accompanied by abnormalities in specific cortical regions and in the adjacent subcortical white matter, exacerbating the cognitive deficit. Moreover, coexisting abnormal MRI signal intensity in the posterior limb of the internal capsule is a powerful predictor of motor outcome severity[4].

2.3 Long-term outcome in preterm neonates

Studies performed in children and adolescents born preterm demonstrate that the relationship between impaired cortical and white matter maturation and functional performance observed in the neonatal period persists into later childhood and adulthood. In particular, data from studies from the USA, Europe, and Australia have all revealed poorer educational outcomes in preterm children than in term controls. At school entry, minor developmental impairment is diagnosed in 30–40% of preterm children and major disabilities in almost 20% of preterm children. More than half of these children require special assistance in the classroom, 20% are in special education, and 15% have repeated at least one grade in school. In France, 42% of children born at 24–28 weeks of gestation and 31% of those born at 29–31 weeks needed special health-care support owing to neurological sequelae, compared with only 16% of those born at 39–40 weeks. The intellectual deficits of preterm

subjects can persist also through adolescence and young adulthood[20]. In a study by the Victorian Infant Collaborative Study Group, 14% of extremely low birthweight preterm children (500–999 g) were classified as severely disabled and 15% were classified as moderately disabled at the age of 14 years, compared with 2% of controls who were classified as severely disabled at this age. Finally, when compared with healthy controls, fewer prematurely born young adults continue their education after high school, and fewer have full-time employment or live outside the parental home as adults[21].

2.4 Long-term outcome in preterm neonates with normal brain MRI

With advances in obstetric and neonatal care, contemporary cohorts of preterm survivors commonly display less severe brain injury that does not appear to involve pronounced glial or neuronal loss. Even if these preterm neonates usually present a lower incidence of cerebral palsy, they remain at high risk for milder and later impairment of the neurological functions, comprising cognitive, language and behavioral disorders[22]. The neuropathologic conditions leading to adverse neurodevelopmental sequelae in later life in preterm neonates without any apparent injury to the brain parenchyma are areas of active research and clinical focus.

Data from several meta-analyses point to the need for closer surveillance for neurodevelopment in preterm neonates without visible brain lesions at conventional MRI and the importance of postnatal interventions and follow-up programs [23]. For example, milder form of GMH-IVH (limited to the subependymal lining of the germinal matrix [grade 1] and/or within the ventricle [grade 2]) without any apparent injury to the brain parenchyma, has been demonstrated to potentially cause neurologic impairment at school age. There are limited human studies evaluating the mechanism of such injury on outcomes, but in vitro studies have demonstrated that various blood components have toxic effects in subventricular zone cells and may impair proliferation, differentiation, and migration of oligodendrocyte precursors, thus affecting the white matter integrity and the cortical development [24].

2.5 Conventional Neonatal MR Imaging and neurodevelopmental outcome

Conventional MR imaging plays a crucial role in the identification of structural brain abnormalities and in the evaluation of altered brain growth, thus capturing the effect of preterm birth on the immature brain[25].

Several MR imaging evaluation scales have been developed to define the severity of brain abnormality at term-equivalent post-menstrual age and to predict neurodevelopmental outcome in preterm neonates[11,26,27]. These scoring systems

address cerebral WM and cortical GM development and estimate the full extent of brain injuries, defining the effect of preterm birth on the brain structure and the relationship between MR imaging–defined brain alterations and subsequent neurodevelopmental outcome in preterm survivors.

The conventional MR brain protocol of neonatal imaging includes T1-weighted sequences, T2-eighted sequences, gradient echo (GRE) sequences and Diffusion-weighted imaging (DWI). T1-weighted and inversion recovery sequences provide excellent anatomic information as well as high contrast between gray and white matter. Three-dimensional Turbo Field Echo techniques provide thin sections through the entire brain with a short acquisition time. T2-weighted sequences provide good contrast resolution between gray matter, unmyelinated white matter and myelinated white matter. Gradient echo (GRE) sequences provide increased sensitivity for the detection of T2*-weighted magnetic susceptibility. This is especially important for diagnosing intracranial hemorrhage, which locally distorts the magnetic field because of the presence of the Fe molecule within blood products. Subtle germinal matrix or intraventricular hemorrhage may sometimes only be detectable with the GRE sequence. DWI and the quantitative map of the Apparent Diffusion Coefficient (ADC) are routinely used for evaluating brain lesions in the acute phase. In particular, acute ischemic lesions became easily detectable on DWI sequence because of the greater sensitivity of diffusion imaging to the cytotoxic edema that affect the water molecules diffusivity into the extracellular matrix.

Neonatal MRI studies have shown that the majority of very preterm infants have white matter abnormalities, which include increasing ventricular size, decreasing white matter volume, increasing intensity of white matter signal, and evidence of decreasing myelination[28]. In addition, there is evidence that these findings are useful in predicting long-term neurodevelopmental outcome based on studies that have shown correlation between neurodevelopmental outcome and either seriously abnormal or normal MRI scans at term equivalent age for study cohorts[28,29].

Nevertheless, only using conventional MRI data is demonstrated to be insufficient to predict neurodevelopmental outcome for individual patients. In one study of 167 preterm infants (GA≤30weeks) who had MRI performed at the equivalent of term gestation and underwent a comprehensive neurodevelopmental assessment at two years of corrected age, moderate to severe white matter abnormalities on MRI were predictive of severe motor delay and cerebral palsy at two years of age[30]. However, 7 of 47 patients (15%) with no white matter abnormality had severe impairment and almost half of the 35 patients with moderate to severe abnormalities did not have any evidence of severe impairment. In a subsequent report of 104 of the original

cohort evaluated at four and six years of age, children with any white matter abnormality were more likely to have neurodevelopmental impairment, and those with moderate to severe abnormalities were at risk for the greatest degree of cognitive impairment[31]. However, similar to the findings at two years of age, there were a few children without white matter abnormalities who had poor neurocognitive outcome, and several children who had moderate to severe white matter abnormalities without impairment.

In an NICHD study of 480 extremely preterm infants (GA<28weeks), MRI with conventional sequences obtained between 35 and 42 weeks postmenstrual age demonstrated increasing severity of white matter abnormalities and significant cerebellar lesions were independently associated with adverse outcome (death or neurodevelopmental impairment) at 18 to 22 months corrected age[28]. However, 4 of 98 infants without any white matter abnormality had neurodevelopmental impairment, while 3 of 18 infants with severe MRI abnormalities were unimpaired or mildly impaired. In a follow-up study at six to seven years of age, findings remained consistent that overall cognitive impairment increased with the severity of white matter abnormality, but there remained a significant number of children with severe cognitive impairment (test scores <70 on Wechsler Intelligence Scale for Children), who had normal neonatal MRIs[32].

2.6 Advanced MRI sequences for neonatal brain study

Recently developed MR-based neuroimaging approaches such as diffusion tensor imaging (DTI), susceptibility weighted imaging (SWI), arterial spin labeling (ASL) and functional connectivity MRI (fcMRI) are now providing insight into alterations in structural and functional brain maturation associated with premature birth that were not detectable with other conventional neuroimaging methods. Newer MR imaging techniques offer higher sensitivity to more subtle structural and functional alterations. Thus, they have the potential to provide a better understanding of the anatomic substrate for the increased susceptibility for cognitive difficulties in this high-risk population.

2.6.1 Susceptibility weighted imaging

Susceptibility weighted imaging (SWI) is an advanced magnetic resonance imaging (MRI) technique that renders high spatial resolution, three-dimensional (3D), fully velocity-compensated, gradient-echo MRI images that are exquisitely sensitive for the magnetic properties of blood, blood products, non-haem iron, and calcifications within the brain.

SWI has been proven useful in the evaluation of various paediatric cerebral disorders, such as traumatic brain injury (TBI), coagulopathic or other haemorrhagic disorders, vascular malformations, cerebral infarction, neoplasms, and neurological disorders associated with intracranial calcification or iron deposition. In neonates, SWI has the potential of providing additional, valuable information in perinatal asphyxia/hypoxic ischaemic encephalopathy (HIE) by identification of white and grey matter microhaemorhages, intraventricular haemorrhage, germinal matrix haemorrhage, and dilated/prominent intramedullary veins (SWI venography). In addition, SWI may potentially provide important information about cerebral haemodynamics and tissue viability in neonates affected with ischaemic stroke by the early recognition of brain tissue with critical perfusion[33].

Quantitative susceptibility mapping (QSM) is a relatively new technique that can be obtained from an advanced post-processing of SWI data, that quantitatively measures the spatial distribution of magnetic susceptibility within biological tissues. Since magnetic susceptibility is sensitive to iron and myelin in the brain, QSM can be another imaging technique used as a marker of iron deposition in the gray matter and myelination in the white matter. In the early developmental neural system, iron is an essential trophic factor required for myelination. Iron-containing oligodendrocytes are found near neuronal cell bodies and are particularly abundant within white matter tracks in the neonatal brain. The sensitivity of QSM to myelin and iron provides an exclusive way to investigate the WM maturation in the neonate and infant brain[34].

2.6.2 Diffusion tensor MRI

Diffusion tensor MRI offers unique insights into the microstructure and organization of white matter by probing the random motion of water molecules. This random motion is hindered or restricted in the direction perpendicular to white matter tracts, even in unmyelinated tracts[35]. Microstructural properties of white matter are often described using quantitative diffusion tensor imaging-derived metrics: Fractional anisotropy, Mean, Axial and Radial diffusivity. Fractional anisotropy is a quantitative, unitless measure that describes the degree of anisotropy of diffusion. Fractional anisotropy ranges from 0 to 1, with a value of 0 indicating perfectly isotropic diffusion and a value approaching 1 indicating increased anisotropic diffusion. Low values of fractional anisotropy are typically observed within the cerebrospinal fluid (CSF) whereas high values of fractional anisotropy are found in highly organized white matter. Mean diffusivity, on the other hand, describes the overall diffusion in units of $10^{-3}mm^2/s$. In contrast to fractional anisotropy, the values of mean diffusivity are high in regions of unrestricted

diffusion (such as CSF) and lower in regions of restricted diffusion (such as white matter). Increased fractional anisotropy and decreased mean diffusivity are, therefore, typically associated with higher organization, (pre-) myelination and decreased water content[36] . The Axial and the Radial Diffusivity are also evaluated to describe white matter maturation in post-natal period, reflecting the magnitude of the diffusivity respectively along the main fiber orientation and across the fibers. In particular, lower values of both Radial and Axial diffusivity reflects increased dendritic arborisation and synapse formation. Changes in organization, (pre-) myelination and water content during early brain development make these metrics ideal candidates for the assessment of brain maturation.

Diffusion tensor MRI also offers the possibility of non-invasive delineation of white matter pathways using tractography by following the direction of preferred water diffusion. The delineated pathways can subsequently be used as three-dimensional regions of interest and diffusion metrics within the tracts can be explored to evaluate the white matter maturation in a tract-based analysis.

In addition, Diffusion tensor MRI enables detailed investigation of gray matter maturation. Below 32 weeks of gestation, the cellular architecture of the cortex is dominated by perpendicular radial glia and apical dendrites, which restrict water diffusion parallel to the cortical surface, resulting in nonzero anisotropy. During the third trimester, decreases in cortical mean diffusivity, radial diffusivity and fractional anisotropy reflect increasing cellular density and maturing dendritic cytoarchitecture[35]. Cortical fractional anisotropy declines until around 38 weeks postmenstrual age, with higher initial values and greater rate of change evident in the frontal and temporal poles and superior parietal cortex, and lower values in the perirolandic and medial occipital cortices. This demonstrates a spatiotemporal gradient of cortical maturation thought to reflect developmental processes such as dendritic arborization, glial proliferation, and synapse formation that occur later in higher-order association cortex during the preterm period.

Finally, recent advances in acquisition (high b-value and high angular resolution) and analysis approaches of diffusion data (i.e. neurite orientation dispersion and density imaging (NODDI), fixel-based analysis (FBA), and constrained spherical deconvolution (CSD)), enable a more detailed analysis of white and grey matter microstructure of developing brain, improving the understanding of the neural substrate associated with impaired brain development of preterm neonates[37].

2.6.3 Arterial Spin Labeling

Arterial spin labeling (ASL) is a completely noninvasive magnetic resonance

imaging (MRI) method that uses magnetically labeled blood water as a flow tracer, providing CBF images of the brain. In ASL, the diffusible tracer is a magnetic label applied to arterial blood water molecules, produced by saturating or inverting the longitudinal component of the MR signal at the level of the neck. If all of the label arrives at the capillary bed or tissue at the time of imaging, this results in a T1-weighted signal reduction proportional to CBF, called the tagged image, which is compared with a control image, in which the blood water molecules are not perturbed. There are several strategies of ASL labeling[38]:

- Continuous ASL (CASL) is a labeling method that uses off-resonance radiofrequency (RF) power and gradients to adiabatically invert flowing water in a proximal tagging plane in the neck to maximize SNR, but requires hardware that is no longer available on modern MRI equipment and results in off-resonance effects that complicate volumetric imaging.

- Pulsed ASL (PASL), in which short (5–20 msec) RF pulses are used to saturate a proximal slab of tissue (including the blood water), is more compatible with modern MRI equipment and leads to high inversion efficiency and lower RF power deposition, but generally has lower SNR than CASL methods. The shorter temporal width of the PASL bolus is an additional source of systematic error in CBF quantification.

- Pseudocontinuous ASL (pCASL) has more recently been introduced as a method to achieve high tagging efficiency, uniting the need for a longer temporal tagged water bolus with lower RF energy deposition and compatibility with modern scanners. pCASL has become the labeling method of choice for clinical ASL, based on a recent consensus white paper on this topic[39].

In neonates, ASL has been applied to see changes in perfusion during brain maturation and to see the predictive value of these changes in term-born infants who undergo hypothermia treatment after hypoxic-ischemic injury[40].

2.6.4 Resting state functional MRI

Resting state fMRI can allow the in-vivo exploration of intrinsic neural activity in the developing brain and it can be used to investigate the loss or preservation of function in the developing brain with or without injury. It utilizes the BOLD signal as an endogenous contrast to infer information through hemodynamic changes related to brain activity. Even at rest, the brain is spontaneously active and shows rich intrinsic dynamics, which can be modulated by external stimuli. This intrinsic neural activity can be detected as correlated continuous low-frequency fluctuations

of the BOLD signal in spatially distinct regions of the brain. Specific resting state networks can be readily and reproducibly identified, which spatially replicate functional networks exhibited by the brain over a range of possible tasks, encompassing distinct neural systems, including medial, lateral and dorsal visual, auditory, somatomotor, executive control and default mode networks. The development of resting state networks follows a specific maturational trend from fragmented elements of the adult pattern at 30 weeks postmenstrual age to a pattern that is remarkably similar to those described in adults in preterm infants at term equivalent age. Visual, auditory, somatosensory, motor, default mode, frontoparietal, and executive control networks appear to develop at different rates, with auditory and visual networks being the first to develop[41].

The resting state functional MRI allow also to perform the analysis of the whole-brain connectome integrating distributed neural systems for exploration during development, and providing additional information on brain plasticity following injury and on the neural substrates underlying the complex neurocognitive impairments observed in children who were born preterm. The most common method by which connectome data are analyzed is using measures from graph theory. A graph, or network, is defined by a set of nodes with interlinking edges. In the brain, regions of gray matter are normally defined as nodes and edges linking these nodes can be constructed by several means including assessing structural connections using diffusion tractography or correlating functional activation detected by BOLD signals[42].

3. RATIONALE

Brain lesions in preterm neonates remain an important cause of neurologic disability and represent one of the leading causes of impaired brain development. Nevertheless, also preterm neonates with normal brain MRI or small brain lesions at term corrected age may show atypical development during infancy. The rationale of the project was to evaluate the role of advanced MRI sequences (susceptibility weight imaging (SWI), diffusion tensor imaging (DTI), arterial spin labeling (ASL) perfusion, quantitative susceptibility map analysis (QSM), and resting-state functional MRI (Rs-fMRI)) in detecting early subtle changes that affect preterm neonatal brain, especially in those patients who show no abnormalities at conventional MRI or presented small brain lesions (i.e. low grade germinal matrix-intraventricular hemorrhage). We also aimed to study the prognostic value of advanced MRI sequences in preterm neonates at term equivalent age for neurodevelopmental outcome at 24 months of age.

4. RESULTS

4.1 *Study Population*

Since November 2015 until June 2017, 287 preterm neonates and 108 term neonates underwent MRI study at term corrected age (40±1 weeks). SWI, DTI and ASL sequences were performed in all neonates. Rs-fMRI was performed in 65 preterm neonates and 20 term neonates. Perinatal clinical data were collected for all neonates. Neurodevelopmental data has been evaluated at 2 years old in 175 neonates.

4.2 First year results

During the first year a qualitative analysis of SWI venography was performed to map out the venous drainage anatomy of the germinal matrix region in a large group of neonates when they reached term equivalent age (40th gestational week).

The first anatomical analysis was performed to establish the differences of subependymal veins anatomy between term and preterm neonates with normal brain MRI (50 and 115 neonates, respectively). Subependymal vein anatomy was classified into 6 different patterns (a typical pattern and 5 anatomical variants) using a qualitative approach. This analysis resulted in the manuscript "Variability of Cerebral Deep Venous System in Preterm and Term Neonates Evaluated on MR SWI Venography" that was published in 2016 on the American Journal of Neuroradiology (IF: 3.65). This study was also rewarded with the *Lucien Appel Prize* of the European Society of Neuroradiology (ESNR 2017). Authors: Tortora D, Severino M, Malova M, Parodi A, Morana G, Ramenghi LA, Rossi A.

4.2.1 "Variability of Cerebral Deep Venous System in Preterm and Term Neonates Evaluated on MR SWI Venography"

Introduction

The cerebral deep venous system includes veins that course into the lateral ventricles from the surrounding white matter and basal ganglia and then exit into the transverse fissure, draining into the internal cerebral veins. These veins are characterized by their subependymal location in the lateral ventricles and by their centripetal direction of blood flow. In 1964, Wolf and Huang classified the deep venous system into two main groups: i) the deep medullary veins (DMV) and ii) the subependymal veins (SV). The DMV are small vessels, arranged in wedge-shaped patterns within the white matter of the cerebral hemispheres, directly participating to the drainage of white matter via the SV into the internal cerebral veins. The SV surround

bilaterally the medial and lateral edges of lateral ventricles, and are classified based on the portion of the lateral ventricles in which they lie (Figure 1).

The first anatomical studies described the brain deep venous system based on ex-vivo angiographic planes. Nowadays, magnetic resonance imaging (MRI) may be used as an alternative non-invasive method to characterize the anatomy of cerebral arteries and veins. Several types of angiographic sequences have been developed to unravel the signal of the blood flow in the arteries (arterial MR angiography) and in the veins (venous MR angiography). Venous MR angiography techniques well demonstrate the anatomy of larger vessels, such as the cerebral dural veins, but often fail to depict the blood flow signal in the smaller veins of the deep venous system. On the other hand, a relatively new sequence, the susceptibility-weighted imaging (SWI), may depict small vessels and venous structures rich in deoxygenated blood. Indeed, this three-dimensional fully velocity compensated gradient recalled echo (GRE) sequence uses deoxyhemoglobin as an intrinsic contrast agent, therefore affording in-vivo assessment of even smaller cerebral veins.

The anatomy of the deep venous system is characterized by a great variability that has been ascribed to a rearrangement of the main draining venous of the primitive choroid plexus occurring in the late period of fetal life. This anatomical variability may play an important role in the pathogenesis of brain lesions in the preterm brain. In particular, germinal matrix-intraventricular hemorrhage, the most frequent brain lesion and leading cause of poor neurodevelopmental outcome and motor disability in preterm neonates, has been associated to a number of acquired and congenital risk factors, including peculiarities in the venous drainage through the brain deep venous vessels. The aim of this study was to describe the anatomy of SV evaluated on SWI-venography in three groups of neonates with normal brain MRI: very preterm (gestational age (GA)<32 weeks), moderate to late preterm (32≤GA<37weeks), and term neonates (GA≥37weeks), and to evaluate the influence of preterm birth on the SV development.

Materials and methods

Subjects

The institutional review board approved this retrospective study and waived informed consent.

The brain MRI studies of 248 consecutive preterm neonates and 83 term neonates acquired from January 2012 to December 2015 were retrospectively evaluated. In preterm neonates, MR imaging was performed at term-equivalent age as a part of a

screening program for identification of prematurity-related lesions. Term neonates (gestational age ≥ 37 weeks) underwent brain MRI within five days of birth in order to rule out suspected brain lesions detected at early cranial ultrasound or to evaluate brain involvement after perinatal asphyxia.

Four exclusion criteria were used in this study: i) presence of brain lesions at MRI; ii) history of perinatal asphyxia or any other clinical adverse event; iii) absence of SWI-venography in the study protocol; and iv) poor quality of MR images.

Preterm neonates were then classified based on gestational age into very preterm [GA<32weeks] and moderate to late preterm neonates [32≤GA<37 weeks]. Among all groups of neonates, the pairs of monozygotic twins were selected and their SV patterns were compared to identify possible differences in SV anatomy among neonates with identical genes.

Imaging

MR imaging was performed with a 1.5T whole-body system (Achieva 1.5T X-Series; Philips Healthcare, Best, Netherlands), using an 8-channel dedicated neonatal head array coil. The parents of the neonates provided written informed consent prior to acquisitions.

All patients were fed before MRI examination in order to achieve spontaneous sleep and were spontaneously breathing during examination. The need of sedation to prevent head movement was agreed with the neuroradiologist on the basis of the infant's state of arousal and the quality of images after the first sequence. Hearing protection was used in all patients. Heart rate and oxygen saturation were non-invasively monitored by pulse-oximetry during examination.

All neonates underwent the same MR imaging protocol. SWI data were collected with a 3D, fully flow-compensated FFE sequence using the following parameters: echo time (TE) = 48 ms, repetition time (TR) = 33 ms, 96 slices, flip angle (FA) = 15°, bandwidth (BW) = 140 Hz/px, FoV = 120 x 120, acquisition matrix = 512 x 512, acquisition voxel size = 0.78 x 0.88 x 1.5 mm, and reconstructed voxel size = 0.7 x 0.8 x 1 mm. Parallel imaging (SENSE) with an acceleration factor of 2 resulted in a total acquisition time of 2:57 min.

Qualitative analysis of subependymal veins

Phase 1. A pediatric neuroradiologist with 20 years' experience in neonatal neuroimaging first reviewed all the MR imaging studies using a workstation equipped with a professional DICOM viewer (OsiriX Imaging Software;

http://www. osirix-viewer.com) in order to exclude neonates with brain lesions. Furthermore, an image-quality assessment of the acquired SWI sequences was performed evaluating the general image quality, noise, venous contrast, and the presence of motion artifacts. The selected SWI sequences were translated and rotated into the anterior/posterior commissure (AC–PC) Talairach baseline to standardize the spatial orientation of each brain.

Phase 2. Two neuroradiologists (with 9 and 6 years' experience, respectively), blinded to neonate identity, reviewed independently the SWI sequences selected in phase 1. They identified the SV on the basis of their anatomical location on axial-reformatted SWI slices. The evaluated SV were: i) the anterior septal vein (ASV), ii) the thalamostriate vein (TSV), iii) the direct lateral vein (DLV), iv) the atrial vein (AV), and v) the internal cerebral vein (ICV) (Figure 1).

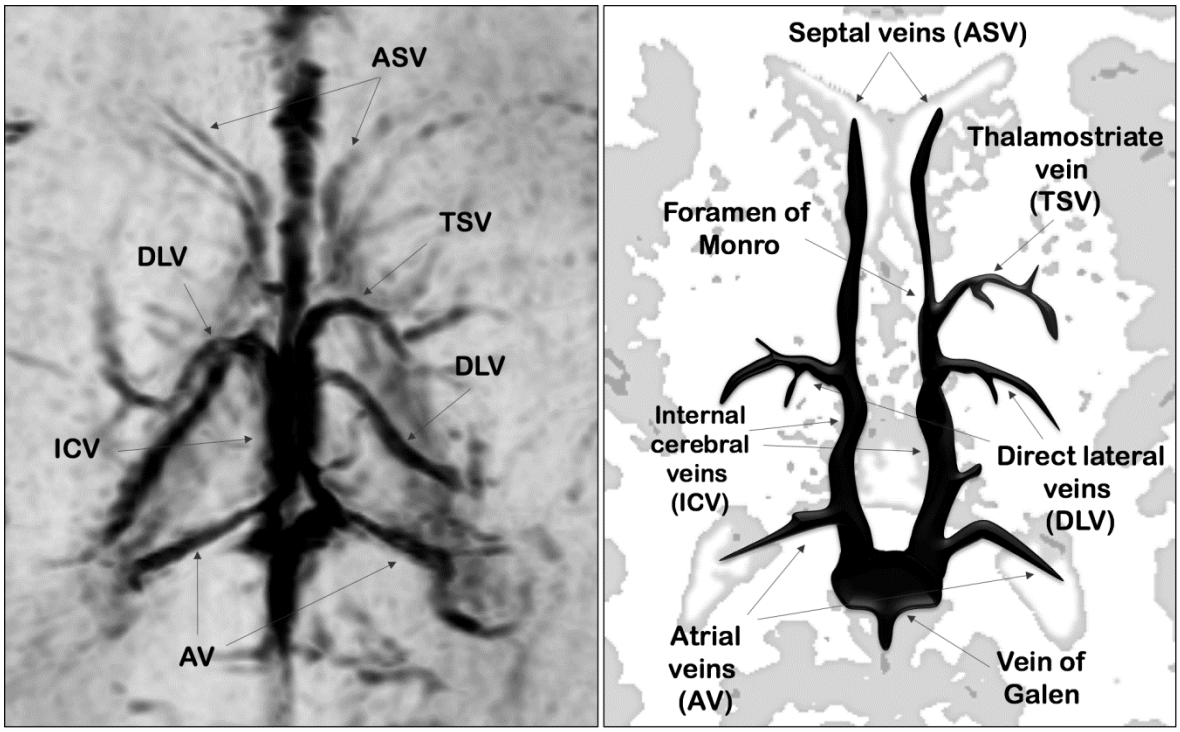

Figure 1 *Axial reformatted SWI venography and corresponding schematic representation of subependymal veins (SV). ASV Anterior Septal Vein; TSV Thalamostriate vein; DLV Direct Lateral vein; AV Atrial vein; ICV Internal Cerebral Vein.*

Subsequently, they evaluated the location of the junction between the ASV and ICV and classified it into two categories: i) at the level of the foramen of Monro, and ii) posterior to the foramen of Monro.

Phase 3. Based on the results of the phase 2 evaluation, readers independently assigned for each brain hemisphere one of the six following patterns of SV anatomy (Figure 2):

- Type 1: the ASV joined the ICV at the level of the foramen of Monro and to the TSV-ICV junction. The DLV was absent. According to Stein and Rosenbaum, this pattern describes the classic anatomy of SV.

- Type 2: the ASV joined the ICV posterior to both the TSV-ICV junction and the foramen of Monro. The DLV was absent.

- Type 3: the ASV joined the ICV close to the site of DLV-ICV junction, posterior to the foramen of Monro. The TSV was absent.

- Type 4: the ASV joined the ICV posterior to both the foramen of Monro and DLV-ICV junction. The TSV was absent.

- Type 5: the TSV and DLV were both present.

- Type 6: the TSV and DLV were both absent.

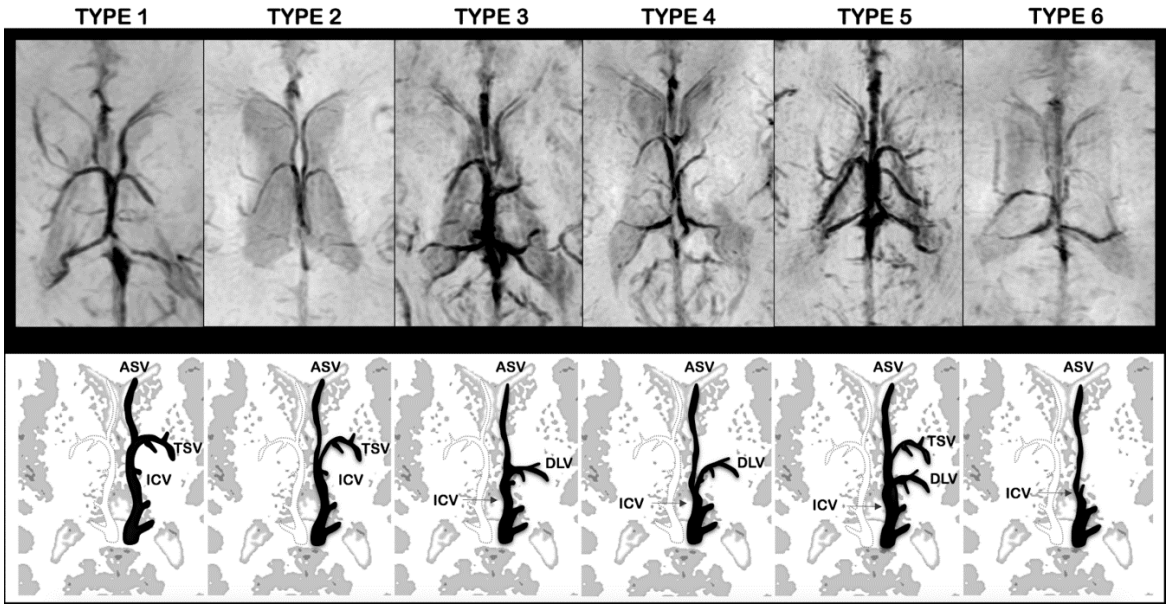

Figure 2 *Axial reformatted SWI venography and corresponding schematic representation of subependymal veins (SV) patterns. The left side of SWI venography and the black schematic vein represent the anatomical pattern.* ***Type 1****: the ASV joined the ICV at the level of the foramen of Monro and to the TSV-ICV junction. The DLV was absent.* ***Type 2****: the ASV joined the ICV posterior to both the TSV-ICV junction and the foramen of Monro. The DLV was absent.* ***Type 3****: the ASV joined the ICV close to the site of DLV-ICV junction, posterior to the foramen of Monro. The TSV was absent.* ***Type 4****: the ASV joined the ICV posterior to both the foramen of Monro and DLV-ICV junction. The TSV was absent.* ***Type 5****: the TSV and DLV were both present.* ***Type 6****: the TSV and DLV were both absent. Atrial veins (AV) were not included in schematic representations.*

In all types of SV patterns, the AV was present and had the same course below the splenium of the corpus callosum, joining the posterior end of the ICV.

Furthermore, the SV pattern of each hemisphere was compared with the contralateral in order to classify each neonate into a symmetric or asymmetric venous pattern group. Finally, the SV anatomical pattern of each pair of monozygotic twin was evaluated in order to assess if a venous "inter-twin" anatomical variability existed.

Phase 4. The same 2 neuroradiologists jointly reviewed the SWI-venography of neonates with Phase 3 discordant evaluation, and were asked to reach a consensus on the SV pattern and interhemispheric symmetry definitions.

Statistical analysis

Statistical analysis was performed by using SPSS Statistics for Mac, Version 21.0 (IBM, Armonk, New York). The level of significance was set at $P < .05$.

The frequencies and percentages of different SV patterns were calculated for all neonates and separately for the three different gestational age groups and for each pair of monozygotic twin. Significant gestational age and gender differences were assessed using Chi-square test. The same test was used also to evaluate significant differences in the distribution of the symmetric and asymmetric SV pattern among the three gestational age groups.

Results

Subjects

The MR imaging studies of 166 patients (133/248, ie 54% preterm neonates and 33/83, ie 40% term neonates were excluded from this study based on the specified exclusion criteria. In particular, 56 neonates presented brain lesions and a pathological clinical history, while 37 studies were affected by motion artifacts and the remaining 73 lacked the SWI-venography.

Thus, the MR imaging studies of 115/248 (46%) preterm neonates and 50/83 (60%) term neonates (13 females, average gestational age 39 weeks, range 37-41 weeks) were eventually included in this study. Eighty-four of 115 (73%) preterm neonates were very preterm (40 females, average gestational age 28 weeks, range 23-32 weeks), and 31 of 115 (27%) were moderate to late preterm neonates (19 females, average gestational age 34 weeks, range 32-36 weeks). Six pairs of female monozygotic twins were identified among the selected neonates: 1 pair was very preterm (gestational age 26 weeks) and 5 pairs were moderate to late preterm neonates (average gestational age 34 weeks, range 32-36 weeks).

Qualitative analysis of the subependymal veins

The consensus reading was necessary in 11/165 (6.6%) neonatal hemispheres (3 very preterm, 4 moderate to late preterm, and 4 term neonates). In all discordant cases, the consensus reading was necessary to define the site of ASV-ICV junction in order to distinguish Type 3 and Type 4 patterns (9/11 hemispheres were finally assigned to the Type 3 pattern).

No gestational age difference was observed between the group of males (N = 91) and females (N = 74) (P=.653). Moreover, no significantly different frequencies of SV patterns were observed between male and female neonates (P=.962).

The frequencies and percentages of each SV anatomical pattern for the three groups of neonates are reported in Table 2. A significant difference was noticed between the six anatomical patterns according to gestational age at birth (X^2= 22.977, P=.011). The classic anatomical pattern (Type 1) was more frequent in term neonates (68%) than in both very preterm (41.7%) and moderate to late preterm neonates (56.5%). The Type 3 pattern was the most frequent anatomical variant, and was more frequent in very preterm (36.3%) and moderate to late preterm (25.8%) neonates. The Type 5 and Type 6 were the less frequent anatomical patterns, and were exclusively observed in very preterm and moderate to late preterm neonates.

Table 1 provides frequencies and percentages of interhemispheric asymmetry of SV pattern for the three groups of neonates. A significant age difference was observed between the symmetric and asymmetric pattern (X^2= 8.194, P=.017). The asymmetric pattern was observed more frequently in very preterm (59.5%) and moderate to late preterm neonates (51.6%) than in term neonates (34%). Furthermore, the right hemisphere of both very preterm and moderate to late preterm neonates more frequently presented the classic SV pattern (Type 1) than the left one. Accordingly, the left hemisphere commonly showed variations from the classic patterns.

The analysis of the SV pattern performed on the 6 pairs of monozygotic twins identified different SV pattern between siblings in 5 out 6 pairs (83.3%).

	VP	MLP	TN	N
Inter-hemispheric Symmetry	34 (40.5%)*	15 (48.4%)§	33 (66%)‡	82
Inter-hemispheric Asymmetry	50 (59.5%)*	16 (51.6%)§	17 (34%)‡	83
TOTAL (neonates)	84	31	50	165

Table 1 *The frequencies and percentages of inter-hemispheric symmetry/asymmetry patterns into the three groups of neonates. VP Very preterm neonates; MLP Moderate to late preterm neonates; TN Term neonates. * indicates percentages of neonates into VP group. § indicates percentages of neonates into MLP group. ‡ indicates percentages of neonates into TN group.*

Discussion

The anatomy of the cerebral deep venous system is highly variable in humans. In adults, a systematic observation of the cerebral venous system on MR images has revealed a great anatomical variability of the deep venous system. Four types of deep venous anatomical variants have been described so far, according to the locations of the ASV-ICV and TSV-ICV junctions in adult brains (Type 1-4). The present study with SWI venography demonstrates that the deep venous system of the neonatal brain shows an even larger spectrum of anatomical variants. In particular, the present classification included two additional patterns characterized by the simultaneous presence or absence of both TSV and DLV (Type 5 and Type 6, respectively). Furthermore, in this classification the posterior location of the ASV-ICV junction relative to the foramen of Monro (Type 3 and 4) was not related to an abnormal course of the TSV, but it was considered an anatomical marker of a prominent DLV.

The presence of such a large number of possible anatomical variants likely reflects the complexity of the development of the deep venous system. Indeed, the evolution of cranial veins falls into an orderly sequence related to the changing environment of the fetal brain. The venous drainage in early stages of brain development occurs through the superficial pial venous network in a centrifugal direction. The

appearance of the deep venous system is concomitant with the expansion of the cerebral hemispheres and seems to be a necessary circulatory adjustment to the thickening of the periventricular white matter, which encourages an additional centripetal blood flow. SV are thought to be derivatives of the primitive choroid veins (superior and inferior choroid veins) that are tributaries of the internal cerebral veins. As the hemispheres expand, complex mechanisms of integration between the draining venous structures of the primitive choroid plexus occur, determining the relatively high frequency of variation of SV in the normal neonatal brain.

To the best of our knowledge, this is the first study using SWI venography to identify and characterize the venous phenotype associated with preterm birth. The analysis of the SV anatomy of preterm and term neonates revealed significant differences. As expected, the most frequent pattern of SV anatomy matched its classical definition (Type 1) in all groups of neonates, i.e. the SV were symmetrical in both hemispheres, and the TSV was present bilaterally with the ASV-ICV junction located near the foramen of Monro. On the other hand, we demonstrated that preterm neonates more frequently presented variations from this pattern. In particular, in very preterm neonates, the DLV replaced a hypoplastic TSV (Type 3 pattern) with higher frequency than in both moderate to late preterm and term neonates (36.3%, 25.8% and 23%, respectively).

The increased variability of the SV pattern in association with preterm delivery may be explained by the modifications of the environment and angiogenetic factors affecting vascular development after birth. In fact, cerebral vessel development is highly influenced by oxygen levels and fatty acid concentrations. Preterm neonates are delivered into a relatively hyperoxic environment compared to the oxygen levels in the uterus, where relative hypoxia stimulates vessel growth and development. In addition, preterm neonates are deficient in numerous factors normally passed over the placenta during the third trimester of pregnancy, including the essential fatty acids, which are structural and functional constituents of cell membranes and play a fundamental role in vascular development and function.

Intriguingly, in the present study the proportions of anatomical variants of SV were equally spread among male and female neonates. Gender differences in brain anatomy are known to be present already at birth. In particular, males have greater intracranial and cortical gray matter volumes than females, and they present larger cranial circumference. The absence of gender differences in the anatomical pattern of SV in the present study further suggests that brain venous development is not only genetically determined, but may also be influenced by perinatal environmental factors. This hypothesis is also supported by the presence of different SV patterns

in almost all pairs of monozygotic twins (83.3%). Similarly, previous MR studies on monozygotic twins showed high variability in the cortical pattern, thus underlying the strong influence of epigenetic factors on central nervous system development.

In the present study, we also found a high age-dependent interhemispheric variability of the SV patterns, with very preterm and moderate to late preterm neonates presenting an asymmetric SV pattern with higher frequency than term neonates. Hemispheric anatomical asymmetries were first observed in postmortem studies on the fetal and premature cortex, showing that some areas of the right hemisphere mature more quickly than the corresponding areas in the left hemisphere. More recent MRI studies demonstrated that left-right hemispheric asymmetries in infants are region-specific. For instance, the superior temporal sulcus develops earlier in the right hemisphere, while the Broca's area develops earlier in the left hemisphere. Recently, Lin et al. demonstrated with Near-Infrared Spectroscopy (NIRS) hemispheric asymmetries and regional differences in cerebral oxygen metabolism, blood flow, and blood volume in premature and term newborns. In particular, they found a higher metabolism and perfusion in the right hemisphere, especially in preterms, supporting current theories about the delay in maturation of the left hemisphere at birth. Interestingly, in the present study, preterm neonates presented the classic SV pattern (Type 1) with higher frequency in the right than in the left hemisphere. Considering that the left hemisphere matures later and is thus more exposed to the influence of postnatal epigenetic factors, we hypothesize that the variations from the classical SV pattern may represent different forms of a delayed venous development, while the Type 1 SV pattern may be considered a marker of maturation of the brain structures. Nevertheless, the relationship among development, morphology and function of the SV itself remains speculative, and is worthy of future investigation. In particular, because the degree of prematurity remains one of the main risk factors for hemorrhagic brain injury, further studies are needed to explore if the wider SV patterns variability of very preterm neonates have implications for the development of these lesions.

Conclusion

MR SWI-venography represents an in-vivo noninvasive method able to describe morphological, positional and numerical variants of SV in neonates. In this study we provided the frequencies of six different anatomical patterns in very preterm, moderate to late preterm, and term neonates with normal brain MRI and demonstrated a significant age difference in SV pattern distribution, likely related

to the influence of the preterm birth and epigenetic factors on deep venous system development.

4.2.2 "Differences in subependymal vein anatomy may predispose preterm infants to GMH–IVH"

A second anatomical analysis on SWI venography was executed to describe features of the subependymal veins anatomy in preterm neonates with low grade germinal matrix-intraventricular hemorrhage (GMH-IVH), exploring the relationship between the anatomical features of subependymal veins and clinical risk factors for GMH–IVH. In this paper a significant difference was noticed among the subependymal veins anatomical patterns according to the presence of GMH–IVH. These anatomical features were significantly associated with GMH–IVH, confirming a potential role of subependymal veins anatomy as predisposing factor for GMH–IVH. This analysis resulted in the manuscript "Differences in subependymal vein anatomy may predispose preterm infants to GMH–IVH" that was published in 2017 on the Archives of Disease in Childhood – Fetal and Neonatal Edition (IF: 3.95). Authors: Tortora D, Severino M, Malova M, Parodi A, Morana G, Sedlacik J, Govaert P, Volpe JJ, Rossi A, Ramenghi LA.

Introduction

GMH-IVH is one of the main complications of prematurity, with important effects on morbidity, mortality and long-term neurological outcome. In particular, severe GMH-IVH is associated with increased short-term and long-term neurologic morbidity, while the long-term neurological outcome of milder form of GMH-IVH is still debated and remains an active area of research. Several studies addressed epidemiology, pathogenesis and risk factors of this multifactorial disease demonstrating that lower gestational age is the most important factor for the development of GMH-IVH. On the other hand, absent antenatal steroid treatment, low Apgar scores, pneumothorax, early sepsis, inherited thrombophilia and the use of inotropic drugs during the first days of life may contribute to GMH-IVH. Despite continuous improvement of perinatal care produced a significant reduction of these acquired risk factors, the incidence of GMH-IVH has not changed accordingly, thus highlighting the importance of structural and connatal factors.

Interestingly, histological studies have provided some evidence that the anatomy of the subependymal veins (SV) may also be implicated in the pathogenesis of GMH-IVH. In particular, it has been hypothesized that the peculiar "U-turn" shape of the

terminal vein may alter blood drainage through the SV near the caudate-thalamic groove, determining an increase of venous pressure in periventricular zones and germinal matrix leading to GMH-IVH. On the other hand, this not recent but very intriguing hypothesis remains unsubstantiated, since the potential role of deep venous anatomy as a contributing factor to GMH-IVH has not been systematically explored so far.

Recently, the development of MR susceptibility-weighted imaging (SWI-venography) has allowed the in-vivo depiction of small veins without the need of a contrast agent, and additionally, has enhanced diagnostic sensitivity in assessment of low-grade brain hemorrhages of neonates.

The aims of this study were to utilize SWI-venography to define the features of SV anatomy in preterm neonates with GMH-IVH, and to compare the SV anatomy of preterm neonates with GMH-IVH with a group of age-matched controls with normal brain MRI. Moreover, the relationships between SV anatomy, GMH-IVH and clinical characteristics were assessed.

Materials and methods

Subjects

For the current study, all very-low-birth-weight preterm neonates (birth weight <1500g) who underwent brain MRI between April 2012 and March 2015 at term equivalent age as a part of a screening program for identification of prematurity-related lesions were retrospectively identified. According to the modified Papile classification, GMH-IVH were classified in: i) grade 1, when the hemorrhage was restricted to the germinal matrix, ii) grade 2, when they were extended into the lateral ventricles, occupying <50% of the ventricular volume, iii) grade 3, when they were characterized by larger amounts of intraventricular blood causing hydrocephalus, and iv) grade 4, when they were complicated by hemorrhagic venous infarction in the periventricular white matter. Neonates were then divided into two groups: i) with GMH-IVH and ii) with normal brain MRI. Four exclusion criteria were used in this study: i) presence of dilated lateral ventricles with distorted SV morphology, related to either post-hemorrhagic hydrocephalus or large periventricular venous infarct, ii) presence of a large intraventricular blood clot hampering the detection of the SV course on the SWI-venography, iii) absence of SWI-venography in the study protocol, and iv) poor quality of MR images.

Imaging

All MRI studies were performed in the Neuroradiology Unit of the Gaslini Children Hospital on a 1.5T scanner, using a dedicated neonatal 8-channel head coil. All patients were fed before MRI examination in order to achieve spontaneous sleep. Hearing protection was used in all patients. Heart rate and oxygen saturation were non-invasively monitored by pulse-oximetry during examination. All neonates underwent the same MR imaging protocol.

Analysis of SWI-venography

MR Images analysis was performed in three different phases.

Phase1. A pediatric neuroradiologist with 25 years of experience in neonatal neuroimaging reviewed all MR imaging studies using a workstation equipped with a professional DICOM viewer (OsiriX Imaging Software; http://www.osirix-viewer.com) in order to perform an image-quality assessment of the acquired SWI sequences, evaluating the general image quality, noise, venous contrast, and the presence of motion artifacts. Furthermore, the same reader identified neonates with normal brain MRI and with GMH-IVH and excluded SWI-venography studies burdened with large intraventricular blood clot and with expanded ventricles.

Phase2. Two neuroradiologists (with 10 and 7 years of experience, respectively), blinded to neonate identity, reviewed independently the SWI sequences selected in phase 1. SV were evaluated on axial-reformatted SWI slices for each brain hemisphere. Based on their anatomical location, the following veins were identified: i) the anterior septal vein (ASV), ii) the thalamostriate vein (TSV), iii) the direct lateral vein (DLV), iv) the atrial vein (AV), and v) the internal cerebral vein (ICV) (Table 1). According to the classification of the SV anatomy proposed by Tortora et al. in neonates with normal brain MRI, readers independently classified SV of each brain hemisphere into six patterns: type 1 was considered as the typical pattern, while type 2-6 reflected anatomical variations. Subsequently, the same 2 neuroradiologists jointly reviewed the SWI-venography of neonates with discordant evaluation and to reach a consensus on the SV pattern classification. Moreover, we tested if the venous anatomy could be correctly identified by a less experienced radiologist, who performed the same analysis on a subgroup of 50 randomly selected cases (100 hemispheres).

SV pattern	Description
Type 1	The ASV joined the ICV at the level of the foramen of Monro and the TSV-ICV junction. The DLV was absent
Type 2	The ASV joined the ICV posterior to both the TSV-ICV junction and the foramen of Monro, resulting in a narrower curvature of terminal portion of the TSV. The DLV was absent
Type 3	The ASV joined the ICV close to the site of DLV-ICV junction, posterior to the foramen of Monro. The TSV was absent
Type 4	The ASV joined the ICV posterior to both the foramen of Monro and DLV-ICV junction, resulting in a narrower curvature of terminal portion of the DLV. The TSV was absent
Type 5	Both the TSV and DLV were present
Type 6	Both the TSV and DLV were absent

Table 1

Phase3. In order to evaluate whether the "U-turn" shape of the subependymal vein close to the caudate-thalamic groove is associated to GMH-IVH, a quantitative measurement of the SV curvature was performed. Such measurement was performed on the TSV in brain hemispheres with the type 1, 2 and 5 anatomical patterns. In type 3 and 4 patterns the curvature degree was measured on the DLV. Neonatal hemispheres presenting the type 6 pattern were excluded from this part of the analysis, since both the TSV and DLV were absent. The same two neuroradiologists traced in consensus a contour line (CL) of 20 millimeters along the vein, focusing on the center of its curved portion, using the segmented line function of MIPAV (Medical Image Processing, Analysis & Visualization version-7.2.0 www.mipav.cit.nih.gov). Then, a straight basal line (BL) connecting the end points of CL was drawn. Vein curvature was quantified using the Curvature Index (CI) defined by the ratio between CL and BL. Higher values of CI correspond to a

narrower curved morphology of the subependymal vein (Figure1). Measurements were repeated 3 times and the mean of these values was used for statistical analysis.

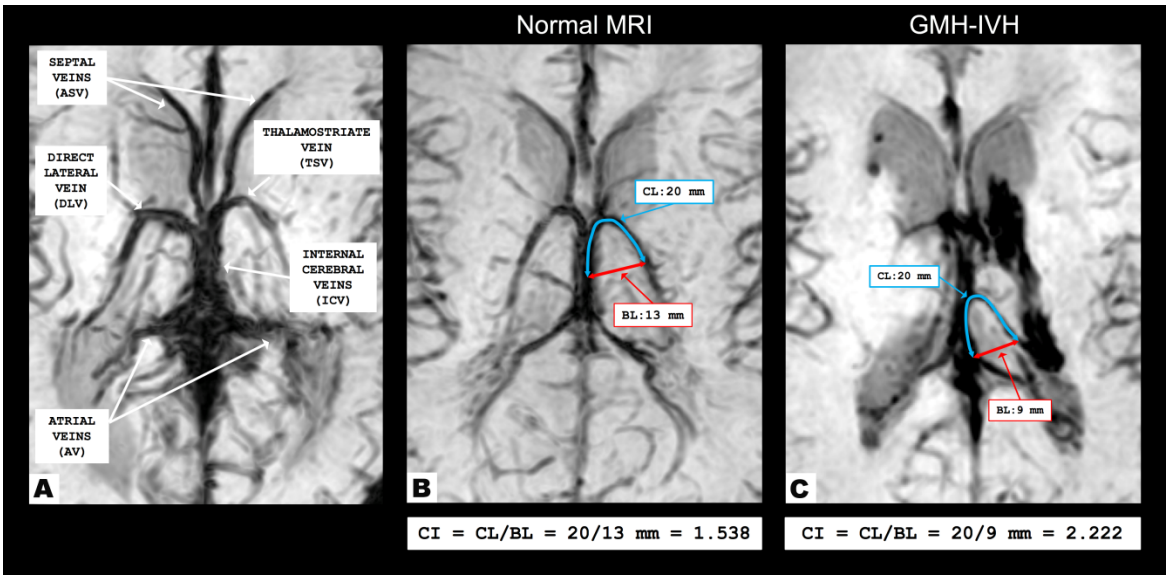

Figure 1 *A) Representation of SV on axial-reformatted SWI-venography. B) and C) Axial-reformatted SWI-venographies in preterm neonates with normal brain MRI (CI measurement performed on TSV) and GMH-IVH (CI measurement performed on DLV), respectively. CL curve line, BL basal line, CI curvature index.*

In order to validate the method of CI measurement, results of the phase 3 analysis were compared with a second set of measurements performed by the same 2 neuroradiologists and by a less experienced radiologist on the same smaller randomly-selected group of 50 neonates (100 brain hemispheres).

Clinical data

Demographic and anthropometric characteristics (gender, birth weight, gestational age), antenatal history (twin gestation, intrauterine growth restriction, antenatal steroids dosage), perinatal variables (type of delivery, Apgar score) and clinical course (respiratory distress syndrome, need for inotropic treatment during first 3 days of life, pneumothorax, patient ductus arteriosus) were recorded for all neonates.

Statistical analysis

Statistical analysis was performed by using SPSS Statistics for Mac, Version 21.0 (IBM, Armonk, New York). The level of significance was set at $P < .05$. Differences between continuous variables were evaluated by Student t and Mann–Whitney U-test, categorical variables were compared by using X^2 test. Cohen's kappa coefficient was calculated to test inter-rater agreement. Multivariable logistic

regression models were used to determine clinical and anatomical factors that were independently associated with GMH-IVH. All variables that were hypothesized to be associated with GMH were entered into the nominal logistic model and then a backward elimination was used to remove nonsignificant independent factors ($P > .05$). In order to evaluate the reproducibility of the quantitative evaluation of CI, a Bland-Altman-plot analysis was performed comparing three sets of CI measurements.

The institutional review board approved this retrospective study and the parents provided written informed consent.

Results

Subjects

The brain MRI studies of 248 consecutive preterm neonates acquired from April 2012 and March 2015 were retrospectively evaluated. The MR imaging studies of 70 patients were excluded based on the criteria mentioned above. In particular, 24 neonates presented dilated lateral ventricles (19 posthemorrhagic hydrocephalus and 5 large periventricular venous infarcts) or large intraventricular blood clot that masked the SV on the SWI-venography, 26 studies were affected by motion artifacts, and in the remaining 20 no SWI-venography was performed for technical reasons.

Thus, the MR imaging studies of 178/248 (71.7%) preterm neonates were included in the study. Forty-eight (27%, 48/178) presented GMH-IVH (21 females, average gestational age 28±2.83 weeks), while 130 (73%, 130/178) had a normal brain MRI (69 females, average gestational age 29.07±2.00 weeks). Fourteen of 48 GMH-IVH neonates presented unilateral hemorrhage (8 exclusively in the left side). Accordingly, 82 GMH-IVH hemispheres (42 left) and 274 normal hemispheres (136 left) were considered for analysis.

Qualitative analysis of the SV

The consensus reading was necessary in 4/356 (1%) neonatal hemispheres (K coefficient=.996; P=.001). In all discordant cases, the consensus reading was required to define the site of ASV-ICV junction in order to distinguish Type 3 and Type 4 patterns (3/4 hemispheres were finally assigned to the Type 3 pattern).

The frequencies and percentages of SV anatomical patterns for each group of neonates are reported in Table 2. A significant difference was noticed between the six anatomical patterns according to the presence of GMH-IVH (X^2=14.242,

P=.014). The classic anatomical pattern was more frequent in neonates with normal brain MRI (50.4%) than in neonates with GMH-IVH (37.8%) (P=.014). Anatomic variants (type 2-6) were observed with higher frequency in neonates with GMH-IVH than those with normal brain MRI (62.2% and 49.6%, respectively). No left-to-right differences were observed (P>.05). In the 14 infants with unilateral GMH-

IVH the venous anatomy on the affected side was characterized by presence of anatomical variations (type 2-6 patterns) in 12/14 cases. In the contralateral normal hemispheres, we found the classic type 1 pattern in 13/14 cases. Therefore, differences in the venous anatomy between the affected and normal hemispheres were overall found in 13/14 cases.

Finally, there was a good agreement between the analysis performed by the pediatric neuroradiologists and the less experienced radiologist (K coefficient =.812; *P*=.001). All discordant cases (6/100) regarded the distinction between Type 3 and Type 4 patterns.

Quantitative analysis of the SV curvature

The assessment of the CI was performed on TSV in 197 hemispheres (39 GMH-IVH) and on DLV in 131 hemispheres (30 GMH-IVH). 28/356 hemispheres with Type 6 pattern were excluded from the quantitative analysis, because TSV and DLV are absent in this pattern. No significant differences were observed between mean CI of TSV and DLV (*P*=.320).

Mean CI of both TSV and DLV was significantly higher in neonates with GMH-IVH both in the left (1.651±0.374 vs 1.422±0.249 for TSV, and 1.681±0.332 vs 1.425±0.338 for DLV) and right hemisphere (1.423±0.274 vs 1.384±0.255 for TSV, and 1.590±0.167 vs 1.384±0.266 for DLV) (Table2).

	Mean TSV CI (*mean±SD*)	**No GMH-IVH**	**GMH-IVH**	**P**
Quantitative analysis	Right	1.423±0.274	1.616±0.155	**.024**
	Left	1.422±0.249	1.651±0.374	**.005**
	Mean DLV CI (*mean±SD*)			
	Right	1.384±0.266	1.590±0.167	<.001
	Left	1.425±0.338	1.681±0.332	.005

Table 2*: TSV Thalmostriate vein, DLV Direct lateral vein, CI curvature index*

Bland-Altman plot analysis did not show significant differences in the two sets of CI measurements performed on the group of 50 randomly selected neonates by two expert neuroradiologists and by the couple of expert and less experienced readers, respectively (mean difference -0.003; standard deviation 0.081; 95%CI -0.0192 to 0.013; *P*=.709 and mean difference -0.052; standard deviation 0.035; 95%CI -0.0182 to 0.032; *P*=.542, respectively)

Relationship between clinical data, venous anatomy and GMH-IVH

To compare the relationship of both the anatomical features of SV and clinical data with GMH-IVH, we performed a multiple logistic regression analysis considering qualitative and quantitative metrics used to evaluate the SV anatomy and all clinical records as independent factors. Independent variables which resulted significantly associated to GMH-IVH are reported in Table 4. GMH-IVH was significantly associated with both the SV anatomical patter (Odds Ratio=2.47, *P*=.0164) and CI (right CI Odds Ratio=4.202, P=.0003; left CI Odds Ratio=2.044, *P*=.0227).

Discussion

The vascular site of origin of GMH-IVH appears to be the prominent endothelial-lines vessels, not clearly arterial or venous, in the germinal matrix. The relative importance of the arterial or venous side of this microcirculation is not fully elucidated. Importance for the role of the venous vascularization was raised by the studies of Takashima et al. who described for the first time the retrograde venous drainage of the germinal matrix, and demonstrated that GMH-IVH occurs at the border zone between the germinal matrix and the adjacent cerebral parenchyma, at the site where germinal matrix venules converge to join the TSV. Indeed, the hypothesis that the morphology of the SV could play a role in the pathogenesis of GMH-IVH was originally introduced in 1964 by Larroche. In particular, the risk of subependymal hemorrhage was thought to be related to venous stasis and thrombosis occurring near the foramen of Monro and caudate head. The importance of the anatomy of the vein in this context was emphasized by Volpe, but to our knowledge no systematic validation has been provided thus far. Therefore, in this study we aimed to qualitatively and quantitatively evaluate the SV phenotype associated with GMH-IVH in preterm neonates using the non-invasive SWI-venography.

Notably, we found a positive correlation between the presence of anatomical SV variants and the occurrence of GMH-IVH in preterm neonates. This association was

further supported by differences in venous anatomy between the affected and normal hemispheres found in neonates with unilateral GMH-IVH, who presented SV variants in almost all affected hemispheres (86%) and the typical SV pattern in the normal sides. Of note, the presence or absence of TSV and its morphology are the key features differentiating the SV variants from the classic pattern[18]. Thus, in the present study, SV variants which mainly differentiate GMH-IVH hemispheres from controls were characterized either by the absence of TSV and DLV (type 6) or by a narrow curved morphology of the TSV (type 2). Therefore, it can be postulated that the absence of both TSV and DLV may influence the venous drainage of the germinal matrix, resulting in a longer course of venules that will drain into the subependymal vein more posteriorly (through the AV) (Figure3 A-B). This peculiar venous drainage may increase the risk for developing venous stasis and venous thrombosis, both known risk factors for GMH-IVH. In addition, developmental immaturity in the cerebral circulation, observed at younger gestational ages due to ongoing angiogenesis and altered vasoregulatory mechanisms, may contribute to the occurrence of GMH-IVH.

On the other hand, we observed a higher incidence of GMH-IVH also in neonatal hemispheres with a narrower curvature of the TSV (type 2) (Figure3 C). Therefore, we used a quantitative approach to investigate if the morphology of TSV or other SV could additionally influence the occurrence of GMH-IVH. Intriguingly, we found that the TSV of neonates with GMH-IVH were characterized by a higher CI of the portions preceding the anastomoses with the ICV. Recently, computational fluid dynamics has been employed to investigate the impact of the vessel curvature on blood flow. These analyses showed that increased vessel curvature leads to flow alterations and increased lumen shear stress which determine venous thrombosis proportionally to the curvature degree. Therefore, we suppose that the narrower curvature of the terminal portion of TSV may cause blood flow alterations and blood congestion in the germinal matrix venular system with a retrograde mechanism, leading to increased pressure on the immature vessel walls and higher risk of venous rupture. This hypothesis is further supported by the well-known correlation between deep venous thrombosis and GMH-IVH, due to a secondary increase of venous pressure in the germinal matrix veins.

Several clinical conditions altering the cerebral circulation in the preterm may lead to increase venous pressure at different levels of the venous system and, accordingly, promotes the occurrence of GMH-IVH. In particular, the respiratory and hemodynamic instability caused by such preterm birth complications (as early pneumothorax or arterial hypotension) may result in wide fluctuations of cerebral blood flow, due to an impaired mechanism of cerebral blood flow autoregulation

and disturbances in the venous circulation. A clear relation among GMH-IVH, pneumothorax and arterial hypotension is well established. Moreover, it has been demonstrated that protection against cerebrovascular events in preterm neonates can be provided by prenatal administration of glucocorticoid, which decreases the severity of the respiratory distress and the incidence of GMH-IVH and stabilizes the existing germinal matrix vasculature. Consistent with these studies, our multivariable logistic regression analysis demonstrated an association of GMH-IVH with pneumothorax, arterial hypotension, and incomplete prenatal steroid administration.

Taken together, these observations support the hypothesis that the vascular architecture of SV may play a role in the pathogenesis GMH-IVH, particularly when clinical conditions affecting the cerebral circulation occur. Nevertheless, the causality between morphology of the SV and the occurrence of GMH-IVH remains speculative and is worthy of future investigation, both in animal models and in human infants.

Among the limitations of this study, we are aware that the neuroradiologists who performed the image analysis were not blinded to the presence or absence of GMH-IVH, easily recognizable on the same SWI-venography sequence. Another limit is that we were obliged to exclude a relatively high number of neonates with GMH-IVH (i.e. 24 cases) thus potentially lowering the statistical power of the analysis. Moreover, we could not evaluate the SV anatomy in preterm neonates with severe GMH-IVH consisted with ventricular dilatation, large intraventricular blood clots, and/or venous infarcts, as they deeply ruin normal venous anatomy. This point could be addressed in future prospective studies using ultrasound with Doppler to evaluate the SV anatomy in the immediate postnatal period, before the occurrence of GMH-IVH. Indeed, new 3D and 4D ultrafast Doppler techniques with extremely high resolution for very small brain vessels have been developed and applied in small animal models, and their promising clinical application is on the horizon.

Conclusions

MR SWI-venography represents an in vivo, noninvasive method able to describe morphologic, positional, and numeric variants of SV associated to GMH-IVH in preterm neonates. Anatomical features of SV may be important predisposing factors for GMH-IVH when clinical conditions affecting the cerebral blood flow occur in the preterm brain.

4.3 Second Year results

4.3.1 "The effects of mild germinal matrix-intraventricular haemorrhage on the developmental white matter microstructure of preterm neonates: a DTI study"

A Track Based Spatial Statistics (TBSS) analysis was conducted on DTI data of a group of preterm neonates (24 neonates) with low grade germinal matrix-intraventricular hemorrhage (GMH-IVH) and no other associated MRI abnormalities on conventional MRI, in order to evaluate the effect of small hemorrhages on the white matter microstructure (assessed by DTI diffusional parameters: Fractional anisotropy (FA), Mean diffusivity (MD), Radial diffusivity (RD) and Axial diffusivity (AD)). The analysis demonstrated that microstructural WM injury can occur in preterm neonates with low grade GMH-IVH even in the absence of overt signal changes on conventional MRI, with different patterns of WM involvement depending on gestational age. This analysis resulted in the manuscript "The effects of mild germinal matrix-intraventricular haemorrhage on the developmental white matter microstructure of preterm neonates: a DTI study" that was published in 2017 in the journal European Radiology (IF: 4.03). Authors: Tortora D, Martinetti C, Severino M, Uccella S, Malova M, Parodi A, Brera F, Morana G, Ramenghi LA, Rossi A.

Introduction

Germinal matrix–intraventricular hemorrhage (GMH-IVH) is a characteristic form of intracranial hemorrhage with multifactorial pathogenesis occurring in premature neonates. The severity of GMH-IVH is commonly described according to the modified Papile classification. Mild GMH-IVH (mGMH-IVH) confirmed with MRI at term corrected age corresponds to early ultrasound diagnosis of hemorrhages restricted to the germinal matrix (grade I) or extending into the lateral ventricles, occupying <50% of the ventricular volume (grade II). Conversely, severe GMH-IVH are characterized by larger amounts of intraventricular blood causing hydrocephalus (grade III) or complicated by hemorrhagic venous infarction in the periventricular white matter (WM) (grade IV).

Although the improvements of neonatal intensive care have led to a significant decrease in the incidence of the severe forms of GMH-IVH, the absolute number of cases remains high due to the increased survival of extremely preterm neonates (PN) and the increased detection rate of minor forms with MRI. Moreover, the spectrum of neurodevelopmental abnormalities related to GMH-IVH has widened, ranging from gross motor and cognitive deficits to milder coordination disorders and lower academic performances, depending on the type and severity of brain damage. In particular, severe GMH-IVH is associated with increased short-term and long-term neurologic morbidity, while the long-term neurological outcome of mGMH-IVH is

still debated and remains an active area of research. Indeed, mGMH-IVH were believed not to increase the risk of neurodevelopmental impairment beyond the risk related to the prematurity alone, until recent studies challenged this notion. Bolisetty et al. demonstrated in a large cohort of extremely PN, that grade I-II GMH-IVH are associated with higher rates of neurodevelopmental impairment at 2 to 3 years corrected age. On the other hand, little is still known on the anatomical substrate of poor neurocognitive and motor outcomes in children with mGMH-IVH. Decreased cortical volume and reduced cerebellar growth at near-term age have been demonstrated in PN with uncomplicated intraventricular hemorrhage. However, despite evidence of disruption of oligodendroglial precursor cells in mGMH-IVH, no diffusion tensor imaging (DTI) studies have explored the microstructural integrity of WM in this condition.

DTI provides useful measures of WM microstructural abnormalities depending on fiber coherence, axonal density, and myelination. Tract-based spatial statistics (TBSS) is an automated, observer-independent approach for assessing the differences of DTI parameters on a voxel-wise basis across groups of subjects, that has been widely used to explore WM microstructural abnormalities in children born preterm.

Here, we hypothesized that WM microstructure of PN with mGMH-IVH and no other abnormalities on conventional MRI differs from that of PN without GMH-IVH, and that these differences may be related to gestational age (GA) with a selective vulnerability pattern. Accordingly, in this retrospective study we aimed to explore differences in the WM microstructure of PN with mGMH-IVH compared to a control group of GA-matched PN with normal brain MRI. Second, we investigated whether selective vulnerability of the WM existed between extremely preterm (GA<29 weeks) and not extremely PN (GA≥29 weeks) with mGMH-IVH. Finally, we explored the relationship of WM microstructural anomalies with neurodevelopmental outcomes at 24 months of age.

Materials and methods

Subjects

The institutional review board approved this retrospective study and the parents provided written informed consent.

All PN (birth weight <1500 g) who underwent brain MRI at term equivalent age between January 2014 and December 2016, in an institutional screening program for identification of prematurity-related lesions, were retrospectively identified. Neonates underwent both an early brain ultrasound study (first postnatal week) and

a routine single-session MRI examination including conventional clinical, susceptibility-weighted images (SWI), and DTI sequences.

Among this population, two groups of neonates were identified: i) with GMH-IVH, and ii) with normal brain MRI. Three exclusion criteria were then considered: i) presence of severe GMH-IVH, ii) presence of brain lesions other than mGMH-IVH, and iii) poor quality of MR images.

Imaging

MRI studies were performed with a 1.5T scanner using a dedicated neonatal head array coil. Parents provided written informed consent prior to acquisitions.

Patients were fed before MRI examination to achieve spontaneous sleep and were spontaneously breathing during examination. Heart rate and oxygen saturation were monitored by pulse-oximetry throughout the examination.

DTI data were acquired along 34 non-collinear directions, with b-values of 0 and 800 s/mm^2 and two excitations.

Qualitative analysis of images

Two blinded pediatric neuroradiologists (AR and MS with 22 and 8 years of experience in neuroimaging, respectively) reviewed in consensus all MRI studies to perform an image-quality assessment. The first step consisted in checking whether all images were imported and sorted correctly and whether the different neonatal DTI studies had the same technical parameters. After this initial examination, a visual inspection of the DTI data was performed to exclude any DTI studies with at least one of these artifacts: (i) signal/slice dropouts, (ii) eddy-current induced geometric distortions, (iii) systematic vibration artifacts, and (iv) ghosting (insufficient/incorrect fat-suppression). Then, readers identified three groups of neonates with: i) normal brain MRI, ii) GMH-IVH, and iii) brain lesions other than GMH-IVH. Neonates with GMH-IVH were finally classified into mild and severe GMH-IVH groups, taking also in account the results of early ultrasound examinations to discriminate between grade I, II and III GMH-IVH. All ultrasound examinations were performed in consensus by two neonatologists (LAR and AP with 29 and 8 years of experiences, respectively) in the acute phases of GMH-IVH.

Structural analysis

Brain segmentation was performed on 3D-T1-weighted sequences calculating gray matter, WM, and cerebrospinal fluid volumes. Non-brain tissue components were removed by using Skull stripping toolbox of BrainSuite v.15c (http://brainsuite.org).

Extracted images were then segmented into tissue classes using unified segmentation as implemented in the "Segment" option of SPM12 (Wellcome Department, University College London, UK). For guiding segmentation, we used tissue probability maps from PN scanned at term age. A neuroradiologist (GM) with 15 years of experience validated brain segmentation results by qualitative assessment. Global brain tissue volumes were extracted from the segmented images of each subject using the Tissue-Volumes function of SPM12. WM volumes were considered covariates for general linear regression models of the TBSS analysis.

DTI analysis

DTI data were analyzed with the FMRIB 5.0.9 software library (https://fsl.fmrib.ox.ac.uk/fsl/fslwiki/). Volumes were registered to the first b0 image, to correct for movement artifacts and eddy current distortions. A brain mask was obtained using BET on b0 volume. DTIFIT was used to fit diffusion tensors to each voxel and compute maps of diffusion metrics: radial diffusivity (RD), mean diffusivity (MD), axial diffusivity (AD), and fractional anisotropy (FA). All maps were aligned to a target in a common space by using an optimized TBSS protocol for neonates providing additional registration steps compared to standard protocol. A mean-FA map and a mean-FA skeleton were finally created for each group. This FA skeleton was thresholded at FA≥0.15 to exclude peripheral tracts with high inter-subject variability and/or partial volume effects with gray matter. Each subject's aligned FA, AD, MD and RD data were projected onto this mean-FA skeleton.

DTI data analysis was performed by using TBSS (http://fsl.fmrib.ox.ac.uk/fsl/fslwiki/TBSS) as implemented in FSL. To evaluate the influence of the GMH-IVH on WM microstructure, differences in FA, MD, RD and AD between neonates with GMH-IVH and with normal brain MRI were assessed. To determine whether a different WM vulnerability to mGMH-IVH existed according to the GA, the same analysis was repeated independently in two groups of neonates: i) extremely preterm (GA<29 weeks) and ii) not extremely preterm (GA≥29 weeks).

Neurodevelopmental outcome

The neurodevelopmental assessment was performed at 24 months of age between January and December 2016, using the Griffiths Mental Development Scales-Revised: Birth to 2 years. Developmental quotient, locomotor, personal-social, hearing-speech, eye-hand coordination, and performance outcomes subscales were assessed by 2 testers (FB and SU, with 19 and 5 years of experience, respectively), unaware of brain imaging findings. In order to evaluate differences in DTI

parameters according to the outcome, for each subscale we used a general linear regression model analysis, applying a correction for multiple comparisons and a cluster-based thresholding (c>3, P<.01). Neurodevelopmental scores lower than 85 were considered abnormal.

Statistical analysis

Continuous variables were summarized as mean, and categorical variables were summarized as frequencies and percentages. Wilcoxon rank test and X^2 test were used to compare continuous and categorical variables between neonates with GMH-IVH and with normal brain MRI.

Since prematurity-related WM changes could influence results of the present study, all TBSS analyses on DTI measures were adjusted for confounding parameters (sex, birth GA and weight, APGAR scores, and total WM volumes) by using a general linear regression model. Two contrasts for each DTI parameter were used to assess for group differences with nonparametric permutation testing via the Randomise function in FSL. Results were corrected for multiple comparisons by controlling the family-wise error rate, using a significance threshold of P<0.05.

In order to confirm the relationship between local WM abnormalities and specific neurodevelopmental abilities, regions of interest were generated from clusters that demonstrated a significance to the TBSS general linear regression model analysis. We implemented a preliminary regression analysis at each region of interest for every DTI measure to remove the potential confounding effect of GA, birth weight, APGAR scores, and WM volumes, considering the neonates who reached the 24^{th} month of life as a single group. We performed power calculation for the general linear regression model analysis considering: i) 5 predictors (each DTI parameter, GA, birth weight, APGAR scores, and WM volumes), ii) the lowest observed R^2 coefficient (equal to 0.34), iii) the probability level of 0.05, and iv) a sample size of 31 neonates who reached the 24^{th} month of age. The lowest observed statistical power was 0.848 (85%). The residual values of the regression, defined as the difference between the actual DTI value from each patient and the simulated normal DTI value at the corresponding GA based on the regression, were then used to substitute for the raw DTI values in the two-tailed partial Spearman rank correlation analysis with neurodevelopmental scores. All statistical analyses were performed using SPSS Statistics software, v21 (IBM, Armonk, NY).

Results

Subjects

Brain MRI studies of 248 consecutive PN were retrospectively evaluated. DTI sequence was performed in 135 neonates. The MRI studies of 32 patients (23.7%) were excluded: 12 neonates presented severe GMH-IVH, 14 neonates presented other brain lesions (11 punctate WM lesions, 2 arteriovenous malformations, and 1 callosal dysgenesis), and in the remaining 6 neonates DTI sequences were affected by motion artifacts. Thus, the MRI studies of 103/135 (76.3%) PN were included in the study, with presence of mGMH-IVH in 24 cases. Thirty-eight (36.9%, 38/103) were extremely preterm (20 females, average GA 26.9±1.8 weeks, 10 mGMH-IVH), while 65 (63.1%, 65/103) were not extremely preterm (34 females, average GA 31.2±2.1 weeks, 14 mGMH-IVH). At the moment of the analysis, 31 neonates had reached 24 months of age, of which 14/31 (45%) were extremely preterm (8 females, average GA 27.2±1.1 weeks, 7 mGMH-IVH), and 17/31 were not extremely preterm (9 females, average GA 30.3±1.8 weeks, 8 mGMH-IVH).

GMH-IVH and WM microstructure alterations

Neonates with mGMH-IVH presented lower FA values in multiple regions compared to controls ($P<.05$): the corpus callosum genu and splenium, superior and inferior longitudinal and fronto-occipital fasciculi, posterior limb of the internal capsule, corona radiata, fornix/stria terminalis, and optic radiations. There were no WM areas with higher FA values in mGMH-IVH neonates than in the control group. Neonates with mGMH-IVH also demonstrated significantly higher RD and MD values in corpus callosum, corona radiata, optic radiations, and anterior fornices. No differences in AD were observed (Figure 1).

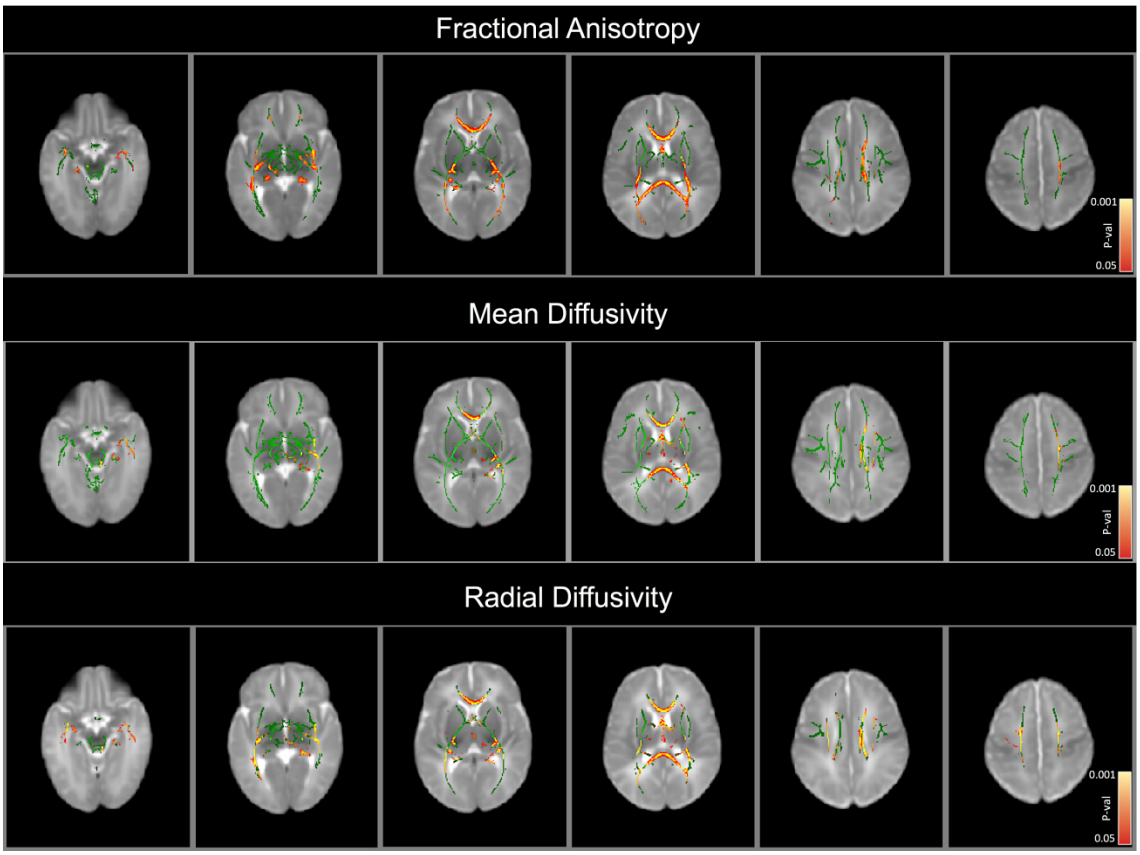

Figure 1 *Green mean FA skeleton overlaid on T2 weighted neonatal template on axial plane. Red-yellow voxels show significant lower FA values, higher MD and RD values in neonates with mGMH-IVH compared to controls (P<.05). No differences in AD were observed.*

Gestational age and WM vulnerability

The comparison between extremely PN with mGMH-IVH and GA-matched controls revealed higher values of MD and RD in the corpus callosum and posterior periventricular WM (Figure 2A-B). Lower values of AD were also detected at level of the corpus callosum (Figure 2C). No differences in FA values were observed.

The comparison between not extremely PN with mGMH-IVH and GA-matched controls revealed lower values of FA in corpus callosum, bilateral internal capsule, optic radiations, inferior longitudinal and fronto-occipital fasciculi and in subcortical frontal WM (Figure 2D). No differences in RD, MD and AD were observed.

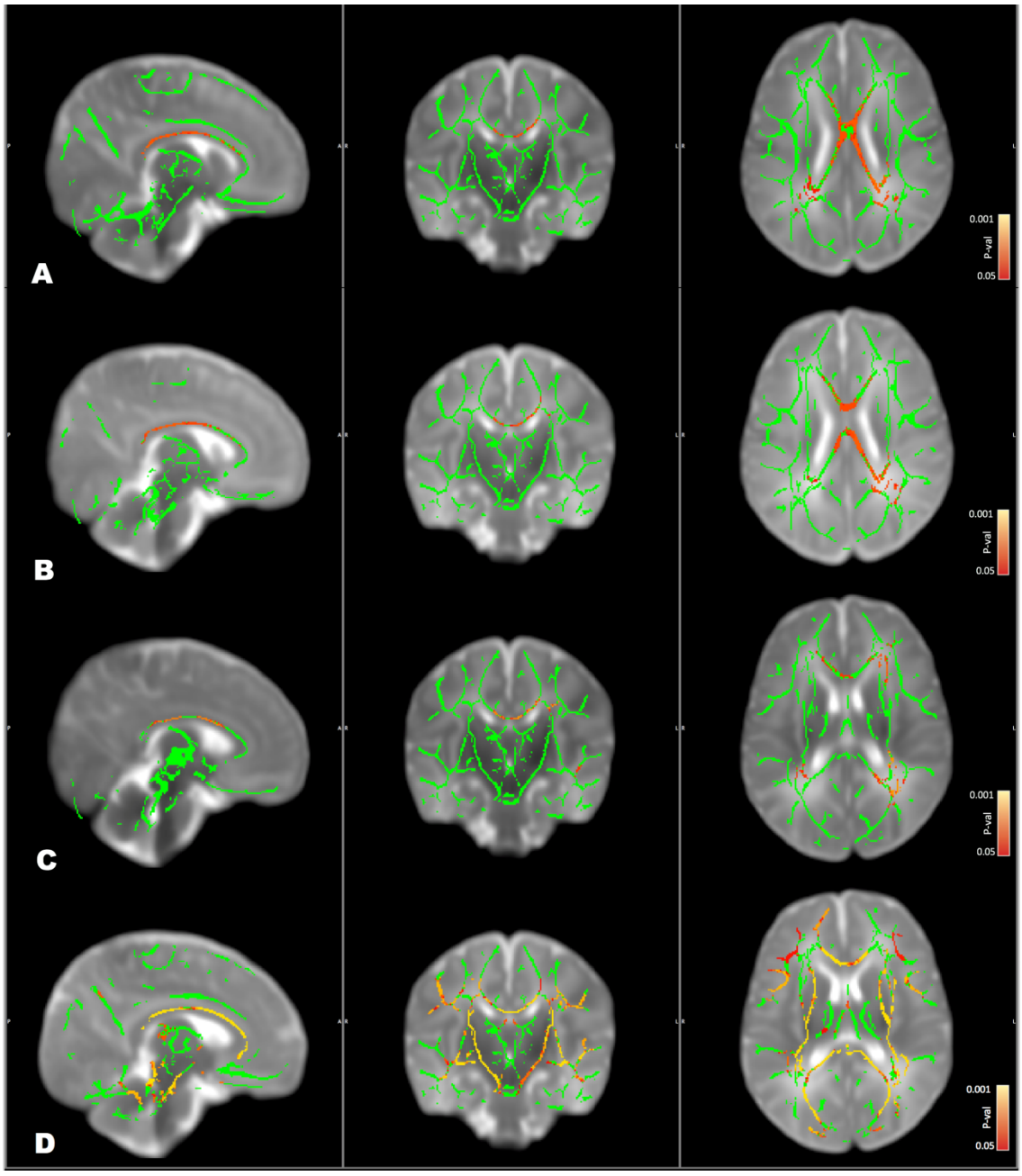

Figure 2 *Green mean FA skeleton overlaid on T2 weighted neonatal template on sagittal, coronal and axial plane. A-B. Red-yellow voxels show significant higher values of MD and RD (respectively) in extremely PN with mGMH-IVH when compared with GA-matched controls. C. Red-yellow voxels show significant lower values of AD in extremely PN with mGMH-IVH when compared with GA-matched controls. D. Red-yellow voxels show significant lower values of FA in not extremely PN with mGMH-IVH when compared with GA-matched controls.*

Neurodevelopmental Outcome and correlations with DTI parameters

Adverse neurodevelopmental outcome occurred more frequently in infants with mGMH-IVH (P=.048) (Figure 3). In particular, among the 31 neonates available for neurodevelopmental assessment at 24 months of age, 17 obtained scores below the cut-off on at least one of the 6 developmental domains of the Griffiths test (11/17 cases with mGMH-IVH), while the performance of the remaining 14 children was within average with age in all domains (4/14 cases with mGMH-IVH).

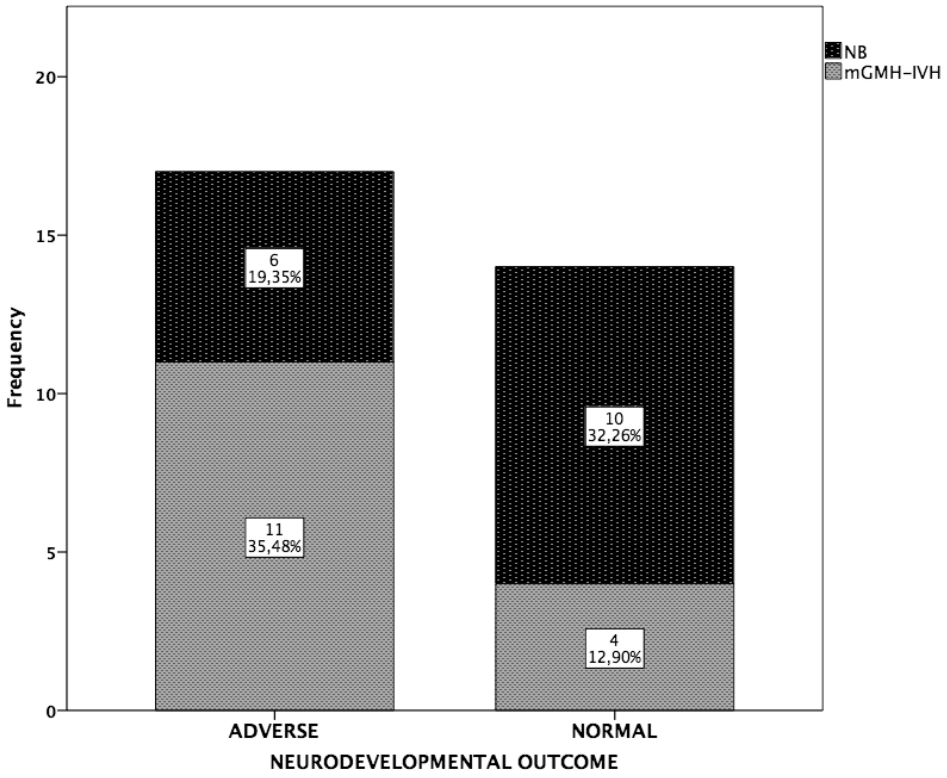

Figure 3 *Frequencies of adverse and normal neurodevelopmental outcome in infants with mGMH-IVH and controls (NB)*

In greater details, there were 10 infants with adverse global developmental quotient (7 with mMGH-IVH, mean score 63,6±4,3), 13 infants with adverse locomotor outcomes (9 with mMGH-IVH, mean score 79,8±6,2), 8 infants with adverse personal-social outcomes (6 with mMGH-IVH, mean score 63,5±11,2), 13 infants with adverse language outcomes (7 with mMGH-IVH, mean score 70,2±12,2), 10 infants with adverse eye-hand coordination outcomes (7 with mMGH-IVH, mean score 52,1±11,2), and 13 infants with adverse performance outcomes (7 with mMGH-IVH, mean score 66,2±9,2). Table1 reports the WM regions where significant correlations between neurodevelopmental subscores and DTI parameters were observed (Figure 4).

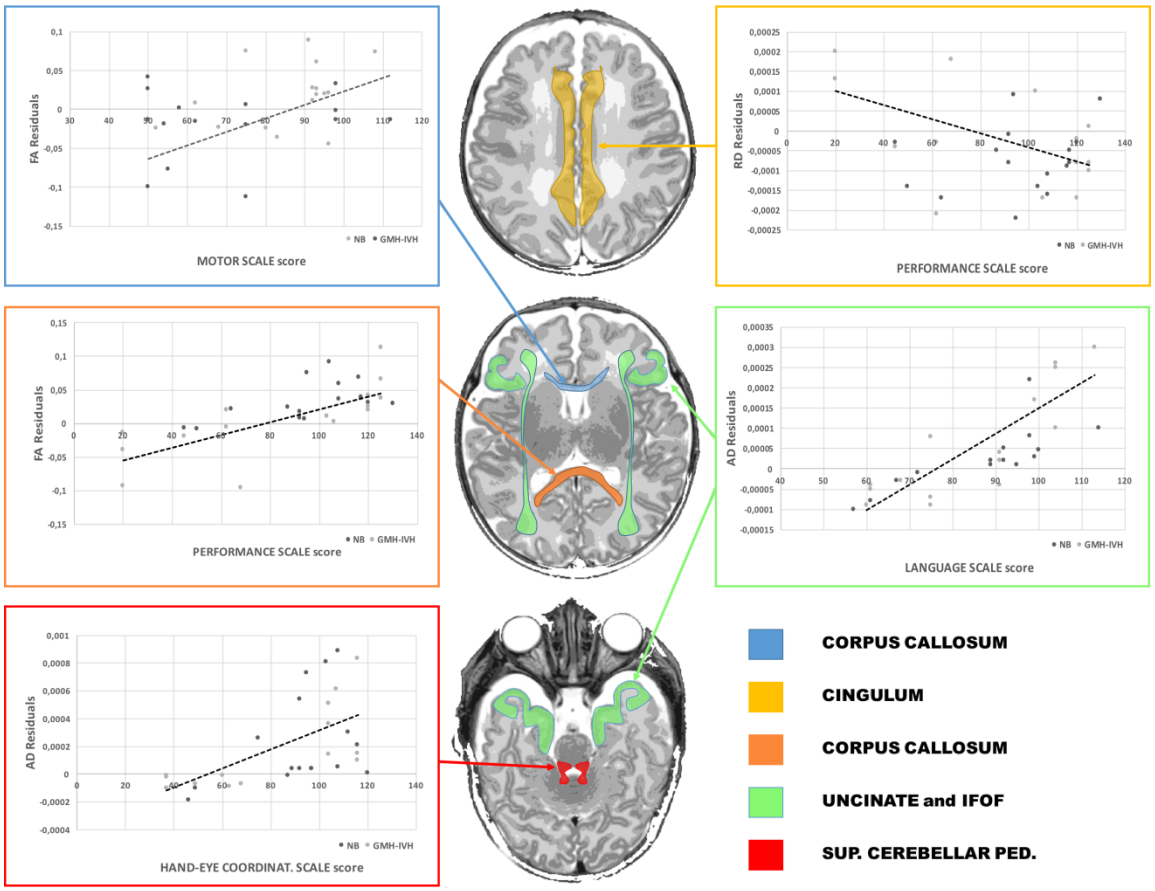

Figure 4 *Diffusion parameters in relation to Griffith's subscale scores. The blue graph demonstrates the relationship between FA residuals and locomotor outcome from voxels in the corpus callosum. The yellow graph demonstrates the relationship between RD residuals and performance outcome from voxels in the cingulum. The orange graph demonstrates the relationship between FA residuals and performance outcome from voxels in the corpus callosum. The green graph demonstrates the relationship between AD residuals and language outcome from voxels in the uncinate fasciculus and IFOF. The red graph demonstrates he relationship between AD residuals and hand-eye coordination outcome from voxels in the superior cerebellar peduncles.*

Discussion

This TBSS-based case-control study unravels abnormal microstructural organization of the WM in PN with isolated mGMH-IVH, and demonstrates a potential relationship of these abnormalities with neurodevelopmental outcome at 24 months in a subset of these babies. In particular, we demonstrated that neonates with mGMH-IVH presented altered DTI metrics in early-myelinated supratentorial WM (i.e. corpus callosum, posterior limb of internal capsule, and optic radiations) when compared with GA-matched controls, even after adjustment for known adverse predictors of outcome. Interestingly, the germinal matrix is the principal source of oligodendroglial precursor cells, which later migrate into cerebral WM in

the third trimester, where they differentiate and produce myelin during the first years of life. We speculate that microstructural WM abnormalities associated to mGMH-IVH may derive from impaired proliferation of oligodendroglial precursor cells in the germinal matrix during the period of occurrence of GMH-IVH (between 25 and 32 weeks of gestation). Of note, previous histological studies on mGMH-IVH showed that even small amounts of blood products and inflammatory compounds are able to suppress the proliferation and differentiation of the oligodendroglial precursor cells. Extracellular hemoglobin and hemosiderin deposition cause cell toxicity following generation of reactive oxygen species such as the hydroxyl radical, damaging proteins, DNA, and cell membranes, and may impair the adjacent WM via direct microglial activation. Decreasing FA and increasing MD and RD in early-myelinated supratentorial WM in PN with mGMH-IVH may thus reflect an early WM damage related to impaired myelination, axonal damage, or abnormal fiber coherence.

Interestingly, we found distinct patterns of WM involvement due to mGMH-IVH, defined by different DTI-based scalar measures, according to the GA. In the affected WM regions of extremely PN with mGMH-IVH, the MD and RD were increased and the AD was reduced, while no differences in FA values were found. Conversely, in not extremely PN, we found prevalent reduction of FA rather than differences in MD, RD or AD. Intriguingly, the simultaneous increase in RD and MD associated to a less pronounced decrease in AD has been observed in other forms of WM degeneration as a result of axonal loss, followed by increase in extracellular matrix and glial cells. On the other hand, isolated decrease of FA in older PN suggests subtle differences in RD and AD, likely reflecting milder microstructural alterations such as minimal fiber loss without gross tissue damage. In the younger premature brain, the cerebral WM is populated mainly by premyelinating oligodendrocytes and oligodendrocyte precursor cells that show a higher vulnerability to excitotoxic and oxidative stress than mature oligodendrocytes. Therefore, we hypothesize that differences in DTI scalar measures may reflect the maturation-dependent vulnerability of WM cells to mGMH-IVH, likely resulting in a more significant WM impairment when occurring at earlier GA.

Another important result of our study was the different distribution of WM changes between extremely and older PN with mGMH-IVH. In particular, in extremely PN, DTI scalar measure abnormalities were observed in the deep-posterior WM (i.e. splenium of the corpus callosum and peritrigonal regions). Conversely, in older PN we detected additional changes at the level of subcortical WM in frontal and temporal lobes. One explanation may be that the site of microstructural WM abnormalities may change according to the maturational stages of microglial cells,

which are abnormally activated by mGMH-IVH. Indeed, microglial activation could be highly damaging to the developing WM, inducing axonal injury and apoptosis through the production of neurotoxins, glutamate, nitric-oxide, and inflammatory cytokines. Notably, before the 30th gestational week, activated microglia density is higher around the germinal matrix and in the subventricular-ventricular zones, both in humans and rodent models. As gestation progresses, microglial cells migrate sequentially through the central WM and cortex along radial glial pathways, WM tracts, and vessels reaching the most anterior and peripheral brain regions. Therefore, the periventricular WM is likely more susceptible to GMH-IVH-related inflammatory changes in earlier GA, while the subcortical WM is more affected in later developmental phases.

Finally, TBSS analysis demonstrated a relationship between the distribution of WM microstructural alterations and specific neurodevelopmental impairments at 24 months of age in a subset of these babies. In particular, altered DTI microstructural measures in the corpus callosum were associated with the poorest motor and cognitive outcomes. This finding is consistent with prior reports demonstrating that mGMH-IVH may affect the macroscopic development of the corpus callosum as well as the cortical gray matter, leading to impaired neurodevelopmental outcomes. Van Kooij et al. demonstrated that cognitive scores at 24 months of age were correlated with FA values in the corpus callosum of PN at term-equivalent age. In addition, as previously demonstrated by Takashi et al., DTI scalar measures abnormalities were observed in the cerebellar WM of PN with mGMH-IVH. Intriguingly, we found a significant correlation between low AD values in the superior cerebellar peduncles and low eye-hand coordination scores, thus underlying the important role of cerebellum in fine movements coordination. Moreover, we found a relationship between FA in the association tracts, including the cingulum and fornix, and the performance score. The fornix is one of the main limbic WM pathways connecting the hippocampus and mammillary bodies, implicated in both executive functioning and memory. Further studies on cognitive functions of PN with mGMH-IVH studied at school age will elucidate whether these DTI measures changes may impact on academic performances.

Limitations of this study include the relatively small sample size, albeit justified by the small incidence rate of isolated mGMH-IVH, and the short neurodevelopmental follow-up performed in the subset of PN aged 24 months at the time of the study. Future investigations of larger populations are awaited to clarify the correlations identified in this study, improving the accuracy of early prognosis for PN with mGMH-IVH. Another limit is that we were obliged to exclude a relatively high number of neonates who, for various reasons (mostly for cessation of sleep or

excessive motion), could not complete a MRI study including a DTI sequence, thus potentially introducing a selection bias.

Conclusion

Microstructural WM injury can occur in PN with mGMH-IVH even in absence of overt signal changes on conventional MRI, with different patterns of WM involvement depending on GA. Moreover, DTI metrics changes in specific WM regions are likely associated to corresponding neurodevelopmental deficits at 24 months of age.

4.3.2 "Prematurity and brain perfusion: Arterial Spin Labeling MRI"

A second analysis was conducted to study and characterize features of brain perfusion in the neonatal period. The cerebral blood flow (CBF) is tightly linked to brain metabolism, and provides another window into neonatal brain development. Further, impaired autoregulation of the CBF is thought to contribute to the development of brain damage in preterm neonates. Accordingly, perfusion-MRI techniques could reveal subtle abnormalities in an apparently normal neonatal brain. Arterial Spin Labeling (ASL) MR imaging non-invasively assesses
brain perfusion and allows a direct quantitative measurement of CBF without administrating contrast material or exposure to ionizing radiation. In this study we demonstrated that ASL could represent a non-invasive method for identifying preterm neonates with a high risk for sub-optimal development, impacting the management of rehabilitative procedures that may be used to reduce sequela.
This research was carried out in collaboration with the Institute of Advanced Biomedical Technologies (ITAB), University of Chieti and with the University of Pennsylvania, Perelman School of Medicine, and resulted in the manuscript "Prematurity and brain perfusion: Arterial Spin Labeling MRI" published in the journal Neuroimage: Clinical (IF: 3.86). This study was rewarded with the *Mario Savoiardo Prize* of the Italian Association of Neuroradiology (AINR 2017).
Authors: Tortora D, Mattei PA, Navarra R, Panara V, Salomone R, Rossi A, Detre JA, Caulo M.

Introduction

Approximately 10-12% of all live births in developed countries are preterm. They are a population at high risk for brain damage and neurodevelopmental disabilities. Improvements in health care for preterm infants have vastly improved survival rates, although comorbid medical and neurodevelopmental difficulties, including cerebral palsy and intellectual disabilities persist. Even in the absence of overt disabilities, a significantly lower percentage of preterms subsequently achieve higher educational and social levels compared to full-terms. As such, the consequences of preterm birth are considered a serious public health issue, especially for very preterm births (gestational age < 32 weeks).
Establishing an association between neurodevelopmental outcome and brain imaging performed around birth would favor earlier treatment strategies to improve long-term outcomes. Currently, there is no accurate method of identifying all preterm neonates at risk of abnormal developmental outcome. Conventional Magnetic Resonance Imaging (MRI) is considered the most sensitive neuroimaging modality for assessing brain myelination and perinatal brain injuries (i.e., cerebral hemorrhage and periventricular leukomalacia). These factors are highly predictive

for subsequent motor abnormalities. However, cognitive and behavioral disorders may occur in the absence of MRI abnormalities (and vice versa) thereby limiting the application of conventional MRI as a predictor of neuro-psychological outcome. Previous studies have focused on the potential role of the advanced diffusion and functional MRI for predicting neurodevelopmental outcome of preterm neonates. Cerebral blood flow (CBF) is tightly linked to brain metabolism, and provides another window into neonatal brain development. Further, impaired autoregulation of the CBF is thought to contribute to the development of brain damage in preterm neonates. Immaturity of both the vascular network and vasoactive signaling in preterm neonates may alter cerebral perfusion pressure, partial pressure of oxygen and carbon dioxide, and neuronal metabolism, thus affecting brain development. Accordingly, perfusion-MRI techniques could reveal subtle abnormalities in an apparently normal brain.

Arterial Spin Labeling (ASL) MR imaging non-invasively assesses brain perfusion and allows a direct quantitative measurement of CBF without administrating contrast material or exposure to ionizing radiation. The primary aim of this study was to compare CBF as measured with ASL MRI in three different groups of neonates (preterm neonates without brain lesions at MRI (PN), preterm neonates with periventricular white matter lesions at MRI (PNp) and term neonates with normal MRI (TN). A secondary aim was to evaluate the correlation between global and regional CBF and clinical outcomes in PN.

Materials and Methods

Patients

The institutional review board approved this prospective study. The brain MR imaging acquisitions of 49 consecutive PNs acquired from January 2011 to December 2013 within five days of term-corrected age as part of an ongoing screening of preterm neonates (study approved by the Ethics Committee of our University and Local Health Authority) were included in this study. The parents or legal guardians of the neonates provided written informed consent prior to acquisitions. A control group of 15 consecutive TN, who showed periventricular hyperechogenicity at routine early cranial ultrasound without asphyxia at birth, underwent an MRI exam within five days of birth. Eleven of the 15 TN who did not show brain lesions at MRI exam and presented a normal neurological status at the twelve-month follow-up visit were enrolled in the study.

MR Imaging

MR imaging was performed with a 3T whole-body system (Achieva 3.0T X-Series; Philips Healthcare, Best, Netherlands) using an 8-channel head receiver array. Neonates were fed and sedated with 0.05 mg oral Midazolam per kilogram of body weight immediately prior to initiating acquisitions. During the scan, neonates were laid in a supine position and swaddled in blankets. Molded foam was placed around the body of the neonate to minimize head movement. Ear protection was always used and consisted of commercially available neonatal earmuffs (MiniMuffs; Natus Medical, San Carlos, California) and adapted ear-canal plugs. Heart rate and oxygen saturation were monitored during the MR imaging session by an intensive care neonatologist with eight years of experience (RS). All neonates underwent the same standard clinical MR imaging protocol.

ASL was implemented using signal targeting and alternating radiofrequency (EPISTAR) with pulsed arterial spin labeling and a multi-slice single-shot echo planar imaging (EPI) readout with parallel imaging (SENSE factor = 2.3) and the following settings: TR/TE, 400/20 ms; flip angle, 40°; matrix size, 80 × 77; FOV, 240 × 240 mm; slice thickness, 6 mm; 14 axial sections with a 0 mm gap; 30 label/control pairs; total scan time, 4.08 min; 100 mm labeling slab thickness of with a gap of 20 mm; and 1250 ms label delay.

MR Data Analysis

A neuroradiologist (MC) with 10 years of experience in neonatal neuroimaging blinded to grouping reviewed the MR imaging studies of all neonates using a workstation equipped with a professional DICOM viewer (OsiriX Imaging Software; http://www. osirix-viewer.com). The T1 and T2-weighted axial images were evaluated in order to establish the presence and location of punctate or cystic white matter lesions typical of PN.

Punctate white matter lesions were defined as T1 hyperintense regions in the periventricular white matter with a diameter of less than 5 mm that did not necessarily present a corresponding decreased signal intensity on T2-weighted images. Cystic white matter lesions were described as T2 hyperintense and T1 hypointense periventricular roundish areas. Since dead cystic tissue is generally not perfused, neonates with multiple white matter lesions and greater than 5 mm of axial diameter were not enrolled.

ASL data analysis

A preliminary image-quality assessment of the acquired ASL sequences was performed evaluating the general image quality, noise (quantitatively), and the presence of artifacts.

The ASL data processing toolbox ASLtbx was used. The toolbox included preprocessing steps of tag and control ASL series realignment, motion correction, coregistration with T1-anatomic sequence, smoothing and brain masking for excluding out-of-brain voxel (Figure 1). The standard toolbox was modified to incorporate the standardized hematocrit values for each individual subject. Quantitative estimates of the regional CBF were performed using the cerebral blood flow maps and the formula described by Ze Wang et al.

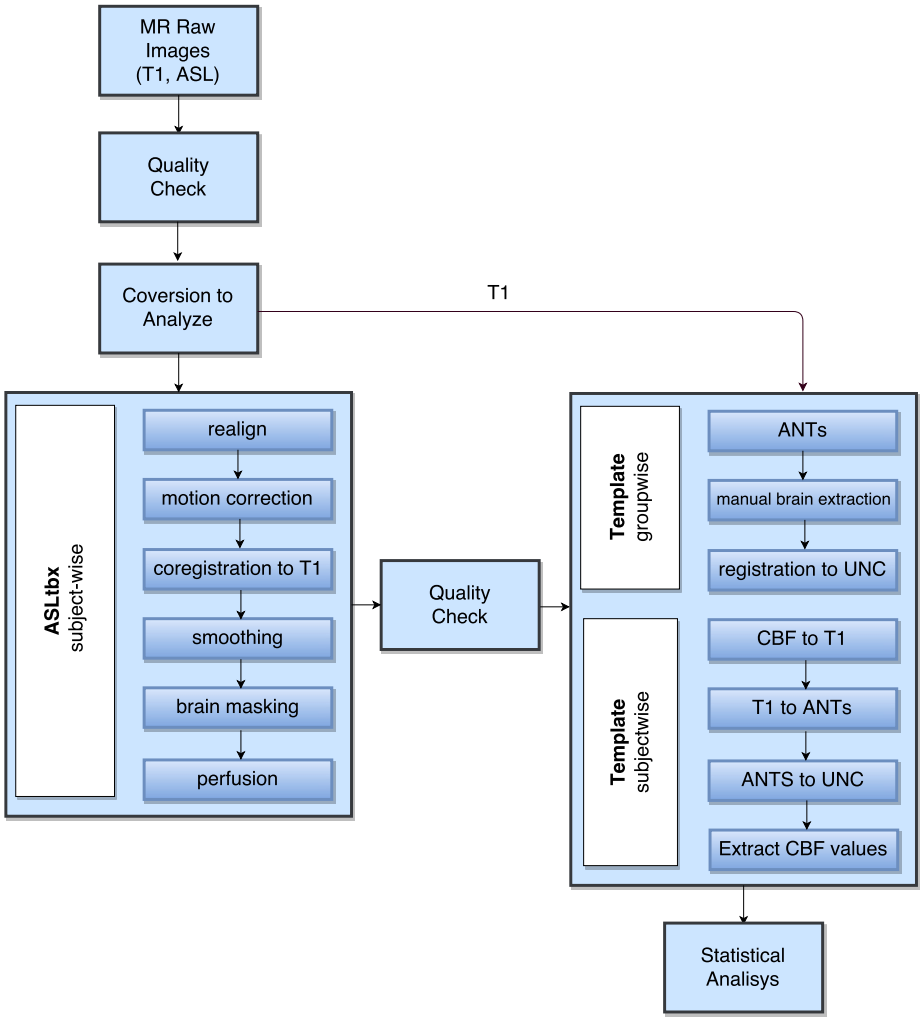

Figure 1. *Flowchart of the pipeline used for ASL data analysis.*

The resulting perfusion weighted images were inspected visually (blinded to group) for residual motion artifacts and subjects with severe artifacts were excluded. A manual segmentation process was used to delineate the boundaries of ventricles and

main arterial vessels (anterior, middle and posterior cerebral arteries) in order to exclude these regions from subsequent analysis.
The segmentation of the brain in gray, white matter and lobes was performed in different steps: an anatomical template that includes T1-weighted sequence datasets of all neonates was built using the Anatomical Normalization Tools (ANTs) Template construction pipeline, then the MR-ASL sequence of each subject was recorded to the template through a nonlinear registration process using the FMRIBs Linear Image Registration Tool (FLIRT) of FSL. Subsequently, the extracted brain with removal of the scalp was registered to the 0-atlas (neonates) of the UNC Infant 0-1-2 Atlases developed by the Biomedical Research Imaging Group of the University of North Carolina School of Medicine. The segmentations provided with this atlas were used to segment the registered perfusion maps for group analysis.
Probabilistic segmentations from International Consortium for Brain Mapping (known as the ICBM database) linearly recorded in UNC 0 atlas space, were used to determine CBF of the whole brain and of the gray matter of each lobe (frontal, parietal, temporal, occipital), cerebellum and basal ganglia. The highest segmentation threshold was applied (99%).

Neuromotor Outcome
Neurologic examinations of the neonates were routinely performed at 12 months of age by a pediatric neurologist who was blinded to the MRI results. Neonates were classified according to the World Health Organization development scale into three groups: 1) “normal” (normal neurologic examination findings); 2) “mildly abnormal” (mild hypertonia, hypotonia, and/or asymmetry); and 3) “definitely abnormal” (severe hypertonia, cerebral palsy).

Statistical Analysis
Statistical analysis was performed with SPSS Statistics for Mac, Version 21.0 (IBM, Armonk, New York). The level of significance was set at $P < .05$. A False-discovery-rate (FDR) correction for multiple comparisons was applied.
Significant group differences in gray and white matter CBF in each brain lobe were evaluated with a linear mixed-model analysis. In order to evaluate the influence of gestational age, a non-parametric correlation test between gestational age and perfusion data was performed. The mean CBF values in each brain region of neonates of different groups were compared with the Mann-Whitney U test.
The presence of a relationship between the neuromotor outcome at 12 months and the CBF values was tested in the preterm group using logistic regression with a backward stepwise conditional method.

Results

The ASL acquisitions of 37/49 (76%) PNs did not show residual motion artifacts at the final image-quality analysis and were included in the study. 8/37 (22%) PNs (2 females; 7 “early” preterms (gestational age<32 weeks); average postmenstrual age at MRI, 40.1± 0.9 weeks; range 39-41 weeks) presented periventricular white matter lesions at MRI (PNp group). 6/8 PNp presented T1-hyperintense punctate white matter lesions (four in both frontal and parietal lobes and two in parietal lobe) and 2/8 PNp showed cystic white matter lesions (major axial diameter < 2 mm) in the parietal lobes.

The remaining 29 PNs (16 females; 16 “early” preterms; average postmenstrual age at MRI, 39.8± 1.2 weeks; range 38-41 weeks) showed no alterations at MRI (PN group). 11 TN without brain lesions at MRI (six females; average postmenstrual age at MRI, 40.8± 0.5 weeks; range 40-42 weeks) were included in the analysis as a control group (TN group).

Brain perfusion

The linear mixed-model analysis showed a statistically significant difference in mean CBF measured in the gray matter of each group of neonates (*P*=.004). No statistically significant hemispheric differences in CBF were observed in any group (*P*=.855) or between the “early” and “late” PN in the PNp and PN groups (*P*=.090). Comparison of means indicated that the CBF of the whole brain of PN was significantly higher than TN (*P*=.011). This difference remained significant when considering the frontal (*P*=.038), parietal (*P*=.002), temporal (*P*=.030), occipital (*P*=*.041*) and cerebellar gray matter (*P*=.010), separately (Figure 2).

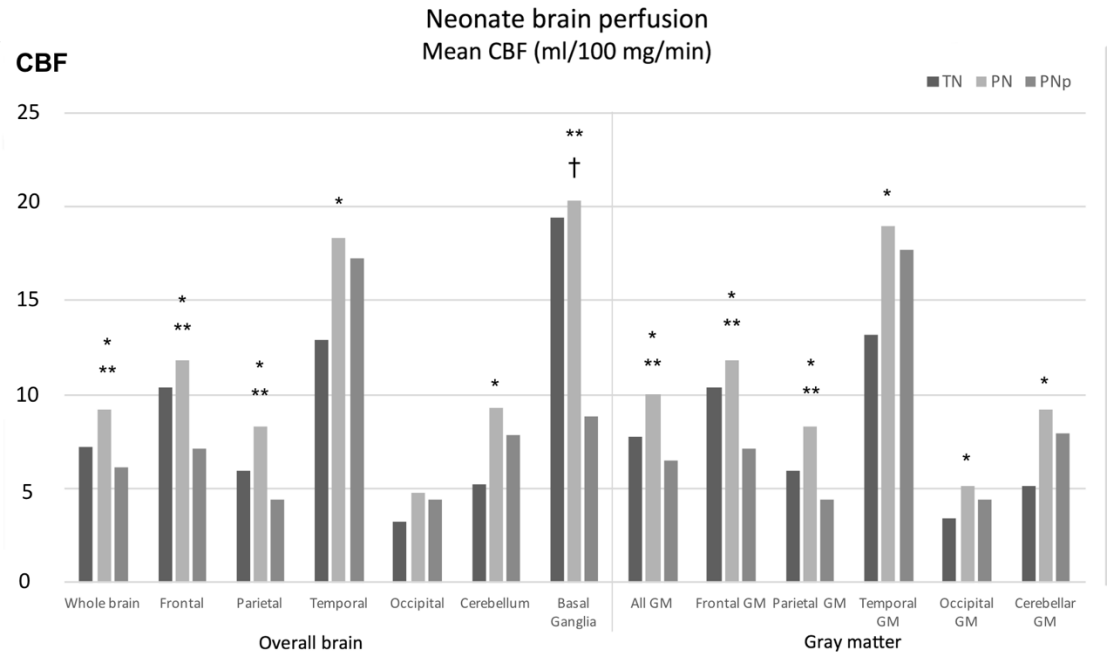

Figure 2. *Regional mean CBF (ml of blood/100mg/min) in the three groups of neonates (Dark gray: TN, Lite gray: PN, Gray: PNp). * PN vs TN; † PNp vs TN; ** PN vs PNp P<.05.*

Comparison of means indicated that the CBF of the whole brain of PNp was significantly lower than PN (*P* =.013). The difference also remained significant when considering the frontal (*P*=.006), and parietal (*P*<.001) gray matter and the basal ganglia (*P*<.001) separately (Figure 1). Finally, PNp showed significantly lower CBF in the basal ganglia when compared with TN (*P*=.004) (Table 2) (Figure 3).

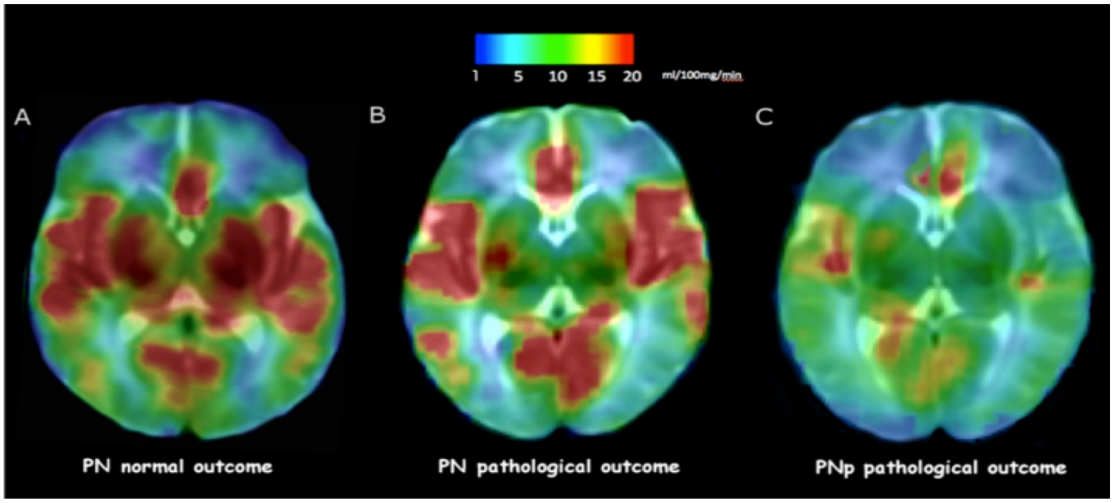

Figure 3. *ASL maps of three preterm neonates. A) and B) CBF maps of two PN who presented normal and abnormal outcome respectively, showing reduced perfusion of basal ganglia in B. C) CBF map of a PNp neonate showing a global reduction of brain perfusion. Color scale indicates CBF (ml/100mg/min).*

Brain regions	Neonate group									p			
	TN			PN			PNp			MLM	M-W	M-W	M-W
	Median	Min	Max	Median	Min	Max	Median	Min	Max		PN vs TN	PNp vs TN	PN vs PNp
Whole brain	7.18	4.04	11.55	9.20	5.72	12.61	6.13	2.13	10.32	.004	.011	.492	.013
All GM	7.72	4.41	12.83	9.98	6.36	13.86	6.53	2.30	11.10	.002	.011	.492	.008
Frontal	10.36	5.88	17.18	11.81	7.38	18.27	7.15	2.72	15.43	.003	.041	.310	.006
Frontal GM	10.38	5.88	17.20	11.82	7.38	18.28	7.16	2.72	15.40	.003	.038	.310	.006
Parietal	5.96	2.04	9.30	8.33	3.89	13.27	4.41	2.45	8.19	<.001	.002	.351	<.001
Parietal GM	5.96	2.03	9.31	8.33	3.89	13.28	4.41	2.45	8.19	<.001	.002	.351	<.001
Temporal	12.88	7.37	27.03	18.37	5.49	30.43	17.24	2.15	26.14	.266	.033	.492	.414
Temporal GM	13.21	7.65	27.80	19.01	5.57	31.82	17.68	2.19	26.75	.243	.030	.492	.373
Occipital	3.27	1.32	8.31	4.73	2.21	12.70	4.43	0.90	6.61	.107	.079	.952	.221
Occipital GM	3.41	1.31	8.42	5.10	2.39	11.68	4.41	0.97	6.42	.058	.041	.904	.158
Cerebellum	5.18	2.85	15.12	9.30	2.65	14.33	7.85	2.21	12.27	.168	.010	.442	.148
Cerebellar GM	5.15	2.75	14.81	9.18	2.78	14.27	7.95	2.22	12.02	.161	.010	.441	.148
Basal ganglia	19.40	13.42	35.88	20.33	11.85	29.10	8.83	1.39	20.25	.001	.952	.004	<.001

Table 2. *Regional median and range of CBF (ml/100g/min) in the three group of neonates. (MLM: linear mixed model analysis; M-W: Mann-Whitney U test; FDR-corrected)*

Relationship between CBF and Neuromotor Outcome

Neuromotor outcomes at 12 months are reported in Table 3. In PNp the presence of white matter lesions was highly predictive of an abnormal neuromotor outcome at 12 months (100% of neonates). Therefore, we focused our attention on the relationship between CBF and neuromotor outcome of PN, which was the only group that presented a highly heterogeneous neuromotor outcome. PN with an adverse outcome ("definitively abnormal" and "mildly abnormal" outcome) showed significantly lower CBF in the basal ganglia compared to PN with "normal" outcome (17.5±4.3 *vs* 22.2±4.8 ml/100mg/min) (*P*=.012) (Figure 4).

	Definitively abnormal	Mildly abnormal	Normal	Lost to follow-up
	Severe hypertonia, Cerebral palsy	Mild hypertonia	Healthy	
TN	0/11 (0%)	0/11 (0%)	11/11 (100%)	0/11 (0%)
PN	0/29 (0%)	10/29 (34.5%)	15/29 (51.7%)	4/29 (13.8%)
PNp	7/8 (87.5%)	1/8 (12.5%)	0/8 (0%)	0/8 (0%)

Table 3. *Clinical outcome results.*

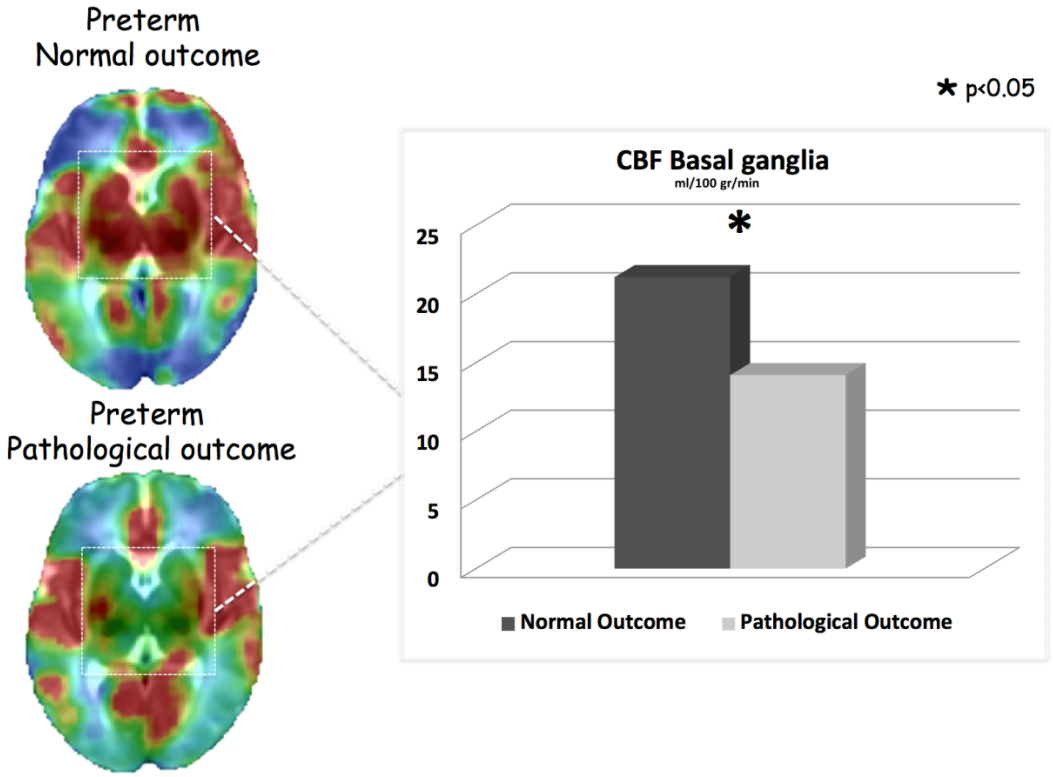

Figure 4. *PN presenting pathological outcome at 12 months showed lower CBF values in the basal ganglia region. The CBF of the basal ganglia resulted to be an independent predictive factor for neuromotor outcome at 12 months in the PN group.*

To evaluate whether CBF of PN was predictive of the neuromotor outcome, a logistic regression analysis was performed and the CBF of all lobes except basal ganglia were removed in a backward stepwise analysis. Mean basal ganglia CBF was an independent predictive factor for neuromotor outcome in PN at 12 months (odds ratio=0.494 95% CI, 0.315-0.785; P=.002). The correlation analysis excluded a confounding effect of the gestational age of PN on the regression analysis results (*P*>.05).

In order to translate these results to a clinical setting, two neuro-radiologists jointly positioned a circular VOI with a 3 mm radius for each lenticular nucleus (right and left) using axial-reformatted 3D T1-wieghted FFE weighted passing through the genu of the internal capsule. Perfusion was then measured on co-registered ASL sequences and the mean of the two VOIs for each patient was used in a ROC analysis. The results were statistically significant (*P*=.037) with a lower threshold (12.2 ml of blood /100 ml of tissue per minute) but with similar sensitivity (88.9%) and specificity (50.0%) as those obtained for the more time consuming group analysis based on automated segmentation.

Discussion

In this study, brain perfusion measured non-invasively using ASL MRI was assessed in three groups of neonates: preterms without brain lesions, preterms with periventricular white matter injury and term neonates with normal conventional MRI. The results showed that PN with a lower ASL-measured CBF in basal ganglia had a worse neuromotor outcome at one year of age.

Our results indicated that the CBF of the whole brain of PN was significantly higher than in TN. The higher CBF of PN is likely related to their greater postnatal age compared to TN (42±22 and 5±2 days, respectively). De Vis et al. demonstrated that CBF progressively increases during the first period of life as synaptogenesis, myelination, and brain functional activity progress. Miranda et al. observed that MR-ASL cerebral perfusion was significantly higher in preterm neonates studied at term corrected age than in the term neonates, indicating that brain perfusion may be influenced by developmental and postnatal age. In addition, our results were concordant with the findings of previous PET and Xe-CT studies that reported an association between higher brain perfusion and metabolism with increasing postnatal age.

Higher CBF was observed in the parietal, temporal and occipital lobes and in the cerebellum of PN as compared to TN. This likely reflects the intense cellular maturation and synaptogenesis associated with the development of sensory (for

example, auditory) systems and motor function. This concept is reinforced by other studies demonstrating that the volume of these lobes increase exponentially during the first months of life. On the other hand, CBF in the basal ganglia did not differ between PN and TN. This region also had the highest CBF, suggesting earlier prenatal maturation compared to the cortex. The lack of a significantly different CBF of the basal ganglia between PN and TN supports the hypothesis that at term-equivalent age the perfusion of these regions has already reached a more advanced stage of maturation, regardless of the gestational age at birth.

PVL are an MRI-detectable white matter lesions typical of PN and the principal pathogenic factors that induce PVL development include hypoperfusion of deep white matter end zones and maternal infection/inflammation. In this study PNp showed significantly lower values of CBF compared to PN, especially in the frontal and parietal lobes and in basal ganglia. This finding could be the consequence of the previously demonstrated neuronal/axonal loss in preterm neonates. A neuropathological study performed on 41 preterm infants indicated that neuronal loss and gliosis were most common in the thalamus, caudate and putamen of infants with white matter lesions. In this study white matter perfusion was not evaluated due to the limits of using ASL to accurately measure this compartment which have been amply reported in literature.

The presence of MRI lesions indicative of PVL in PN studied at term represents an important predictor of both poor neuromotor outcome and cognitive delay during the preschool and early school years. However, even PN without PVL may develop neuropsychological deficits. In the present study, all PNp presented an adverse neuromotor outcome at 12 months but more than a third of the PN also developed neuromotor deficits. These findings demonstrate that in PN the absence of white matter abnormality on MRI is not fully predictive of a normal outcome (low specificity). However, a positive correlation between CBF in the basal ganglia and neuromotor outcome was found in PN.

Our findings differ from the results of recent studies that demonstrated hyperperfusion in the brain of term neonates with hypoxic-ischemic encephalopathy (HIE). The differences were probably the consequence of the different time that elapsed following insult. That is, hyperperfusion reported after HIE is considered an acute hemodynamic compensation attempt induced by perinatal hypoxia-ischemia, whereas the hypoperfusion in PNp indicates a chronic phase of brain injury.

The evolution of regional brain perfusion and metabolism during the period of postnatal growth may correlate with the development of neuroanatomical structures and functional maturation. Therefore, the higher CBF in the basal ganglia of PN with normal outcome could reflect a more advanced stage of brain development.

But, the lower CBF values of basal ganglia of PN with abnormal outcome support the hypotheses that prematurity influences the autoregulation of brain perfusion, contributing to the delayed maturation of brain. This observed selective effect on the basal ganglia is in accordance with their advanced development around birth and the greater involvement following perinatal asphyxia.

This finding needs to be replicated in a larger series but, if verified, it has the possibility of identifying PN at high risk for sub-optimal neuropsychological development using ASL perfusion at term-corrected age could significantly impact their management by identifying the infants who require medical/rehabilitation therapy. Post-hoc evaluation of results obtainable by manually positioning VOIs indicated that basing a prognosis on the perfusion of the basal ganglia in a clinical setting is valid. Therefore, the results of this study can be easily translated into a clinical setting allowing patient evaluation in a sufficiently short time period; i.e., before the patient is removed from the scanner.

The main limitation of this study was that the only clinical finding that was consistently available from patient records was the neuromotor outcome at 12 months. In addition, the number of PN enrolled precluded a more detailed statistical analysis; specifically, the definition of a CBF threshold able to distinguish PN with normal and adverse neuromotor outcome with high diagnostic accuracy.

Another limitation of this study regards the use of a PASL sequence has been reported to have a lower image quality when compared with other ASL perfusion sequences (i.e., pCASL) for the study of neonates. However, the recommended quality assurance steps were applied while determining the best delay time for our scanner/study population/sequence characteristics using a multiphase sequence. The validated PASL settings for quantitatively evaluating neonatal brain perfusion provided adequate grey matter SNR. Furthermore, a significant percentage of ASL acquisitions of our population was excluded from the analysis due to the motion artifacts. In this study, tag-acquisition delay time was also not corrected for individual hematocrit but a standardized hematocrit correction was applied.

Since ASL perfusion is highly susceptible to head movements, a preliminary quality check of the images should be performed immediately after the acquisition of the sequence and studies affected by motion artifacts could be repeated during the same examination.

Multicenter studies with larger sample sizes will be required to further refine the cut-off but the identification of the area of interest for modifications of perfusion is an important first-step.

Conclusion

This study demonstrated differences in cerebral perfusion between PN and TN. PN showed higher CBF compared to TN and PNp. PNp showed a global reduction of brain perfusion. Also, CBF in the basal ganglia of PN was positively associated with neuromotor outcome at 12 months and could represent a non-invasive method for identifying PN with a high risk for sub-optimal development. The ability to identify PN at risk of sub-optimal neuromotor development could greatly impact the management of rehabilitative procedures reducing sequela.

4.4 Third year results

4.4.1 "Quantitative susceptibility map analysis in preterm neonates with germinal matrix-intraventricular hemorrhage"

During the last year a quantitative analysis was performed to evaluate in vivo the effects of germinal matrix-intraventricular hemorrhage (GMH-IVH) on the magnetic susceptibility of several brain regions in preterm neonates studied at term equivalent age, using a Magnetic Resonance Quantitative Susceptibility Analysis (MR-QSM).
A recent ex-vivo study revealed extensive amounts of extracellular hemoglobin and its catabolic products in the periventricular white matter of preterm rabbit pups 72 hours after intraventricular hemorrhage. The extracellular hemoglobin released during ongoing hemolysis within the intraventricular space diffused passively through the ependyma driven by concentration gradients, migrating in the white matter in directions of less restricted diffusion (Ley D. 2016). In our study we hypothesized that similar mechanisms may occur even in human preterm neonates during the acute phase of GMH-IVH, and that post-hemorrhagic iron overload in the periventricular white matter may be responsible of the cascade of lipid peroxidation and free radical formation that promote oxidative and inflammatory injury of the neonatal brain. Because ferritin and hemosiderin are the major source of non-heme iron deposition in the human brain, and they induce strong variation in brain magnetic susceptibility, MR-QSM analysis represents an unique tool enabling the quantification in vivo of brain iron overload due to blood products accumulation.
This study demonstrated that paramagnetic susceptibility changes occur in several periventricular white matter regions of neonates with severe GMH-IVH compared with controls, likely related to the accumulation of hemosiderin/ferritin iron following diffusion of large amounts of intraventricular blood products into the brain parenchyma.
Results of this analysis were published in the Journal of Magnetic Resonance Imaging (IF:3.61): "Quantitative Susceptibility Map Analysis in Preterm Neonates With Germinal Matrix-Intraventricular Hemorrhage". Authors: Tortora D, Severino M, Sedlacik J, Toselli B, Malova M, Parodi A, Morana G, Fato MM, Ramenghi LA, Rossi A.

Introduction

Germinal matrix-intraventricular hemorrhage (GMH-IVH) is a frequent form of intracranial hemorrhage occurring in premature neonates with important effects on morbidity, mortality and long-term neurological outcome. The germinal matrix is a highly vascular, developmentally dynamic structure in the subventricular zone, containing multiple cell types, such as premigratory/migratory neurons, glia, and neural stem cells. Rupture of the fragile germinal matrix capillaries may occur in response to both congenital and acquired factors, including venous anatomical variants, low birth weight, altered cerebral blood flow, increased venous pressure, or hypoxic-ischemic injury. According to the modified Papile classification, mild GMH-IVH corresponds to hemorrhages restricted to the germinal matrix (grade I) or extending into the lateral ventricles, occupying < 50 % of the ventricular volume (grade II). Conversely, severe GMH-IVH is characterized by larger amounts of intraventricular blood causing hydrocephalus (grade III) or complicated by hemorrhagic venous infarction in the periventricular white matter (grade IV).

The effects of GMH-IVH on brain development are still under investigation. Even though the cause of the primary lesion is easily identified on MRI by the presence of blood products, the exact extent of the injury may not be recognizable with conventional sequences. Thus, several advanced MR techniques have been used to explore the structural modifications occurring in brain of neonates and children with GMH-IVH. Vasileiadis and colleagues revealed decreased cortical volume at near term age in preterm neonates with uncomplicated IVH (i.e. without parenchymal involvement or posthemorrhagic hydrocephalus). Tam and colleagues demonstrated decreased cerebellar volume associated with supratentorial IVH as a result of concurrent cerebellar injury or direct effects of subarachnoid blood on cerebellar development. More recently, MR diffusion tensor imaging was used to evaluate white matter microstructural changes in preterm neonates with mild GMH-IVH, providing evidence of a gestational age-dependent selective vulnerability in several white matter regions, correlating with adverse neurodevelopmental outcome at 24 months.

Quantitative susceptibility mapping (QSM) is a relatively new MRI technique for quantifying the spatial distribution of magnetic susceptibility within biological tissues, including iron, calcium, myelin, deoxyhemoglobin, and blood degradation products. This technique utilizes phase images, solves the magnetic field to susceptibility source inverse problem, and generates a three-dimensional susceptibility distribution. Recently, QSM has been used to study brain development in neonates, evaluating the susceptibility contrast between gray and white matter derived from brain myelination. Moreover, QSM has been applied in

the standardized quantitative stratification of cerebral microbleeds and neurodegenerative diseases, as well as of accurate gadolinium quantification in contrast enhanced MRI. Indeed, QSM represents an unique tool enabling the identification of brain iron overload due to blood products accumulation, brain ageing and neurodegenerative cascades. An elevated iron milieu causes cell toxicity following generation of reactive oxygen species, with consequent damage to the proteins, DNA and cell membranes. Compared to other advanced techniques, such as brain morphometry and diffusion metrics, QSM thus offers important insights into the underlying mechanisms of several brain diseases.

Here, we hypothesized that the magnetic susceptibility of normal-appearing gray and white matter structures in preterm neonates with isolated GMH-IVH is higher compared to control preterms, accordingly to the GMH-IVH grading. Also, we hypothesized that the magnetic susceptibility of the non-affected hemispheres may be higher in cases of unilateral GMH-IVH. Accordingly, in this retrospective study we aimed at: i) quantitatively evaluating the susceptibility of several white and gray matter regions in preterm neonates with or without GMH-IVH using QSM, ii) assessing differences in magnetic susceptibility related to the severity of GMH-IVH, and iii) quantifying the white and gray matter magnetic susceptibility of hemispheres contralateral to hemorrhage in patients with unilateral GMH-IVH.

Materials and methods

Subjects

The institutional review board approved this retrospective study.

We retrospectively identified all preterm neonates with birth weight <1500 g who underwent brain MRI at term equivalent age in the setting of our institutional screening program for identification of prematurity-related lesions between January 2014 and December 2016. The MRI scans of the brain were performed after written consent of parents or legal guardians. All neonates underwent an early brain ultrasound study during the first postnatal week, that was interpreted in consensus by two neonatologists (LAR and AP with 29 and 8 years of experience, respectively).

We first identified neonates with GMH-IVH and normal brain MRI. In particular, images were reviewed for presence of any white and gray matter signal alteration or brain malformation by a pediatric neuroradiologist (GM with 13 years of experience). Two exclusion criteria were considered: i) presence of brain lesions other than GMH-IVH, and ii) poor quality of MR images due to motion artifacts. Thus, the brain MRI studies of 180 consecutive preterm neonates were retrospectively evaluated.

Imaging

MRI studies were performed with a 1.5T scanner using a dedicated neonatal head-spine array coil (Intera Achieva 2.6, Philips, Best, the Netherlands). Patients were fed before MRI examination to achieve spontaneous sleep and were spontaneously breathing during examination. Heart rate and oxygen saturation were noninvasively monitored. Oxygen saturation ranged between 97 and 99% in all neonates during the examinations. The MRI examinations included conventional clinical and susceptibility-weighted images (SWI). SWI data were collected with a 3D fully flow-compensated fast-field echo sequence by using the following parameters: TR: 48 ms, TE: 33 ms, 96 sections, flip angle: 15°, bandwidth: 140 Hz/px, field of view: 120x120 mm^2, acquisition matrix: 512x512, acquisition voxel size: 0.78x0.88x1.5 mm, and reconstructed voxel size: 0.7x 0.8x 1 mm. Parallel imaging (sensitivity encoding) with an acceleration factor of 2 resulted in a total acquisition time of 2 minutes and 57 seconds. Original phase image data of the SWI scan were stored for later offline QSM reconstruction.

Qualitative analysis of images

Two blinded pediatric neuroradiologists (AR and MS with 25 and 8 years of experience in neuroimaging, respectively) reviewed in consensus all MRI studies to perform an image-quality assessment, including noise, venous contrast and presence of motion artifacts, using a workstation equipped with a professional DICOM viewer (OsiriX Imaging Software; http://www.osirix-viewer.com). Three groups of neonates were identified: i) with normal brain MRI, ii) with GMH-IVH, and iii) with brain lesions other than GMH-IVH. Neonates with GMH-IVH were classified into mild (grade I and II) and severe (grade III and IV) groups, taking into account the results of early ultrasound examinations performed in the acute phases of GMH-IVH to discriminate between grade I, II and III. Moreover, patients with unilateral or bilateral GMH-IVH were identified (Figure 1).

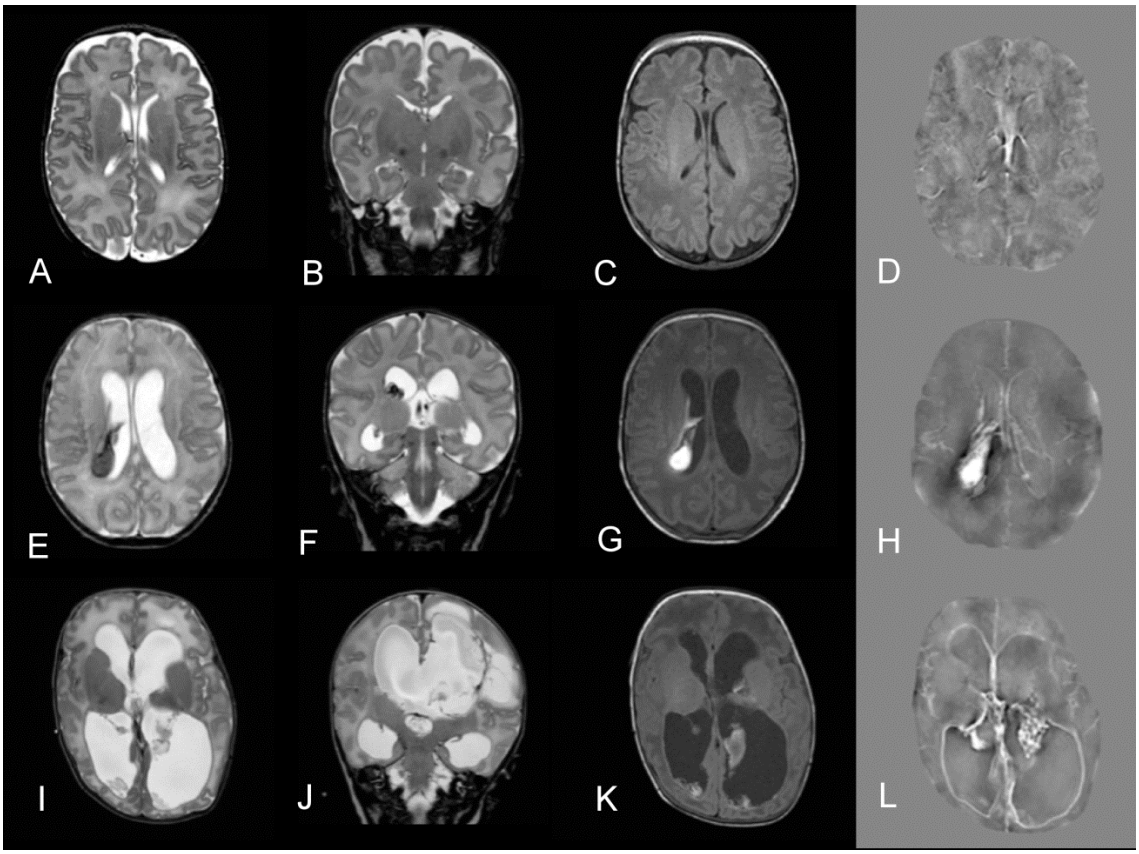

Figure1. *Quantitative susceptibility map analysis was performed on three groups of neonates:*
i) Neonates with normal brain MRI: Axial T2-weighted (A), Coronal T2-weighted (B), Axial T1-weighted (C), SWI (D), and QSM map (E) images of a preterm neonate with normal brain MRI. ii) Neonates with mild GMH-IVH: Axial T2-weighted (F), Coronal T2-weighted (G), Axial T1-weighted (H), SWI (I) and QSM map (J) images show right intraventricular hemorrhage in a preterm neonate with mild GMH-IVH. iii) Neonates with severe GMH-IVH: Axial T2-weighted (K), Coronal T2-weighted (L), Axial T1-weighted (M), SWI (N) and QSM map (O) images show post-hemorrhagic hydrocephalus with left frontal infarction in a preterm neonate with severe GMH-IVH.

QSM analysis

The QSM data was analyzed for each brain hemisphere, thus identifying three groups of hemispheres: i) normal, ii) with mild GMH-IVH, and iii) with severe GMH-IVH. The contralateral hemispheres of patients with unilateral GMH-IVH were excluded from the group of normal brain hemispheres, and were considered in an independent analysis to test if unilateral GMH-IVH may influence magnetic susceptibility of the contralateral hemisphere.

QSM data were reconstructed using custom Matlab code based on the superfast dipole inversion approach. To improve the background-field removal and subsequent QSM reconstruction, we modified the common brain mask erosion process by only excluding voxels with insufficient background-field removal. Such

voxels were identified by showing background-field corrected phase values below 5% or above 95% of the values of all other border voxels of the mask. The background-field corrected phase was than recalculated with the updated mask. This process was iteratively repeated until the standard deviation of the background-field corrected phase values of the border of the mask was below 1.5 times the standard deviation of all background-field corrected phase values within the mask. This brain mask refinement approach resulted into globally more homogeneous background-field corrected phase and, therefore, susceptibility maps. The criteria of the voxel erosion process were established while optimizing the QSM reconstruction framework, balancing the number of eroded voxel in order to maximize the improvement of background field removal and subsequent QSM reconstruction, while obtaining a sufficiently large mask including both white and deep gray matter structures.

Regions of interest (ROIs) identification

To evaluate the brain magnetic susceptibility changes due to GMH-IVH, two neuroradiologists (DT and GM with 5 and 15 years of experience, respectively) placed in consensus 2D regions of interest (ROIs) across multiple contiguous slices on the QSM maps and T2 weighted images to segment the main deep gray matter structures (basal ganglia and thalami) and WM regions (frontal, parietal, temporal, and cerebellar white matter, and centrum semiovale) (Figure 2). The ROIs were manually drawn using MRIcron (people.cas.sc.edu/rorden/index.html), and ranged in size from about 800 to 2500 mm, depending on the size and shape of the different anatomical brain regions, and taking in consideration the eventual loss of brain tissue in patients with severe GMH-IVH. Careful attention was paid to avoid partial volume effects, blood vessels, hemorrhage, hemosiderin deposits, and superficial hemosiderosis. Median values of susceptibility (in part per million, ppm) were extracted from each ROI. The median tissue susceptibility within each ROI was recorded and referenced to the whole brain susceptibility for analysis.

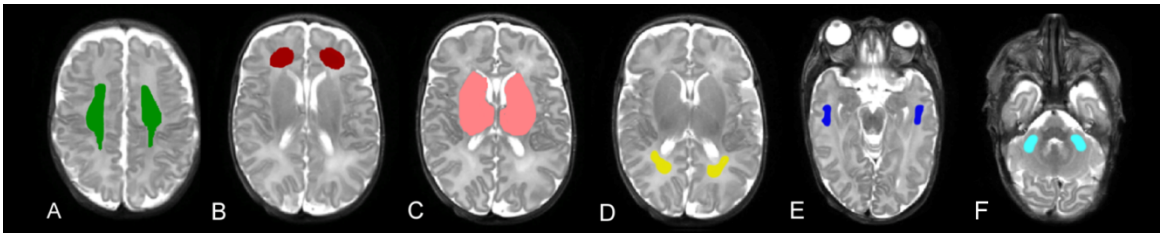

Figure2 *Regions of interest used for the quantitative evaluation of susceptibility*

Statistical analysis

Continuous variables were summarized as median (range), and categorical variables were summarized as frequencies and percentages. Wilcoxon rank and X^2 tests were used to compare continuous and categorical variables between neonates with GMH-IVH and normal brain MRI. For each ROI, a one-way analysis of covariance was utilized to test statistically significant differences of magnetic susceptibility between neonates with GMH-IVH and normal brain MRI, and among the three groups of neonates (i.e. normal, mild GMH-IVH, and severe GMH-IVH), using gestational age at birth and postmenstrual age at MR examinations as covariates. Preliminary checks were conducted to ensure that there was no violation of the assumptions of normality, linearity, homogeneity of variances, homogeneity of regression slopes, and reliable measurement of the covariate. Moreover, estimated marginal means of magnetic susceptibility were used to obtain Bonferroni corrected post-hoc comparisons. The level of significance was set at .05. All statistical analyses were performed using SPSS Statistics software, v21 (IBM, Armonk, NY).

Results

Subjects

A SWI sequence was performed in 164 neonates. The MRI studies of 37 patients (22%) were excluded: 28 neonates presented other brain lesions (18 punctate WM lesions, 6 vascular malformations, and 4 brain malformations), while SWI sequences were affected by motion artifacts in the remaining 9 neonates. Thus, the MRI studies of 127/164 (77.4%) preterm neonates were included. Ninety-two neonates (72.5%; 92/127) presented normal brain MRI; 20 neonates (15.7%; 20/127) presented mild GMH-IVH; and 15 (11.8%; 15/127) neonates presented severe GMH-IVH. Nine neonates presented unilateral GMH-IVH (all mild GMH-IVH, 6 on the left hemisphere). Thus, 184 normal brain hemispheres and 61 hemispheres with GMH-IVH were considered for assessing the magnetic susceptibility differences in neonates with or without GMH-IVH, also taking into account the GMH-IVH grading, while 9 contralateral hemispheres of patients with unilateral GMH-IVH were used to test if unilateral GMH-IVH may influence magnetic susceptibility of the contralateral hemisphere.

QSM data

In preterm neonates with normal brain MRI, the susceptibility values of the 6 white matter and deep gray matter regions were lower than zero, corresponding to the diamagnetic properties of these structures. In neonates with GMH-IVH, higher

positive susceptibility values (i.e. paramagnetic) were observed at the level of centrum semiovale (P<.001), temporal WM (P=.037), and parietal WM (P=.002) (Figure2). No significant differences were found at the level of the basal ganglia, cerebellar WM, and frontal WM. Table 1 reports median susceptibility values measured in the 6 brain regions in neonates with normal brain MRI and with GMH-IVH.

	Group	Median (ppm)	Range (Min/Max)	Number of hemispheres	P
Basal ganglia	No GMH-IVH	-0.0037	-0.0143/0.0065	184	.273
	GMH-IVH	-0.0083	-0.0322/0.1046	61	
Centrum semiovale	No GMH-IVH	-0.0014	-0.0248/0.0195	184	**<.001**
	GMH-IVH	0.0019	-0.0258/0.2854	61	
Cerebellar WM	No GMH-IVH	-0.0007	-0.0371/0.0301	184	.795
	GMH-IVH	-0.0001	-0.0412/0.0344	61	
Frontal WM	No GMH-IVH	-0.0002	-0.0228/0.0316	184	.696
	GMH-IVH	0.0051	-0.1731/0.0502	61	
Temporal WM	No GMH-IVH	-0.0012	-0.0428/0.0221	184	**.037**
	GMH-IVH	0.0011	-0.0689/0.0917	61	
Parietal WM	No GMH-IVH	-0.0001	-0.0398/0.0294	184	**.002**
	GMH-IVH	0.0005	-0.0498/0.2747	61	

Table 1 *Median values of brain susceptibility in brain white matter regions*

Regarding the analysis of brain susceptibility according to the GMH-IVH grading, significant differences were observed among the three group of neonates at the level of centrum semiovale (P<.001), temporal WM (P=.033), and parietal WM (P=.005) (Figure 3). In particular, the post-hoc analysis demonstrated that at the level of the centrum semiovale, patients with severe GMH-IVH had higher magnetic susceptibility compared to both neonates with mild GMH-IVH and controls (P=.005 and P<.001, respectively). At the level of temporal and parietal WM, patients with severe GMH-IVH demonstrated higher magnetic susceptibility compared to controls (P=.028 and P=.007, respectively), while only a trend of higher magnetic susceptibility emerged from the comparison with mild GMH-IVH patients. No differences in magnetic susceptibility were observed between neonates with mild GMH-IVH and controls (P>.05).

Finally, the magnetic susceptibility of the centrum semiovale of the 9 contralateral hemispheres of neonates with unilateral GMH-IVH was higher compared to neonates with normal brain MRI (mean susceptibility of 0.0103±0.0283 ppm and -0.0134±0.0072 ppm, respectively; P=.001).

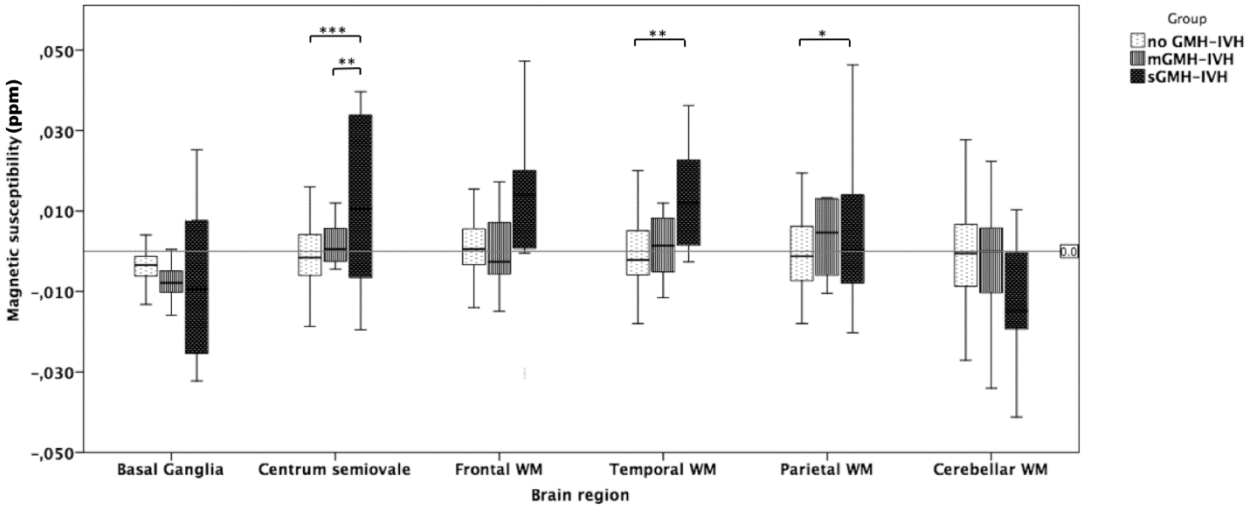

Figure 3 *Comparison of magnetic susceptibility among neonates with severe GMH-IVH (grade III and IV) (sGMH-IVH), neonates with mild GMH-IVH (grade I and II) (mGMH-IVH) and neonates with normal brain MRI (No-GMH-IVH). Median magnetic susceptibility values of centrum semiovale increased significantly in neonates with sGMH-IVH when compared with both No-GMH-IVH and mGMH-IVH neonates. Median magnetic susceptibility values of parietal and temporal WM increased significantly in neonates with sGMH-IVH when compared with No-GMH-IVH neonates. At these levels, only a trend of higher magnetic susceptibility emerged from the comparison between sGMH-IVH and mGMH-IVH. No differences were observed between mGMH-IVH neonates and No-GMH-IVH neonates. (* indicates P<.01; ** P<.001; *** P<.0001). Note: WM: white matter; ppm: parts per million.*

Discussion

In this study, we explored in-vivo the effects of GMH-IVH on the magnetic susceptibility of several brain regions in preterm neonates studied at term equivalent age with QSM analysis. The first finding was that in control preterm neonates the magnetic susceptibility of both white and subcortical gray matter structures was diamagnetic, with values close to zero. As indicated by several recent studies, brain magnetic susceptibility is mainly influenced by myelin in the white matter and by iron deposits in the deep nuclei, evolving both spatially and temporally during the lifespan. Argyridis and colleagues evaluated the temporal evolution of magnetic susceptibility in the white matter of the developing mouse brain: as myelination progressed from the second postnatal day up to 56 postnatal days, the normal white matter magnetic susceptibility gradually became diamagnetic and correlated with

the optical intensity of myelin-stained histological slides. Similarly, Li and colleagues demonstrated in a large group of healthy subjects aged from 1 to 83 years that the white matter magnetic susceptibility first becomes more diamagnetic due to progressive myelination, followed by a continuing decreasing of diamagnetism as the brain ages secondary to demyelinating processes. Conversely, the magnetic susceptibility of deep gray matter regions correlated linearly with the iron content in the globus pallidum, stratum, red nucleus, and substantia nigra. Starting from values close to zero at 1 year of age, the magnetic susceptibility of these regions increased exponentially throughout the lifespan. At the moment, little data is available on the normal magnetic susceptibility of brain structures in children below age 1 year. In 2011, Zhong and colleagues demonstrated lack of gray-white matter contrast in full-term neonates. Accordingly, we found diamagnetic values close to zero in both deep gray and white matter of normal preterm neonates, in keeping with little iron deposits and initial stages of myelination in this age group.

Of note, in the present cohort of preterm neonates, the occurrence of GMH-IVH led to a paramagnetic change of the susceptibility of surrounding white matter structures, namely the centrum semiovale and periventricular temporo-parietal regions, likely induced by the presence of hemosiderin or ferritin iron deposits. Indeed, in vivo estimates of regional brain iron distribution obtained by the QSM approach compared well with postmortem measurements of brain iron concentration. This finding was related to GMH-IVH grading, inasmuch we observed differences in magnetic susceptibility between preterm neonates with severe GMH-IVH and mild GMH-IVH or controls, but not between preterm neonates with mild GMH-IVH and controls. This result may be related to the presence of hemorrhagic hydrocephalus, superficial hemosiderosis or infarction in periventricular WM, rather than with hemorrhages of the germinal matrix alone. Alternatively, we cannot exclude the effects of the relatively small sample size and/or the insufficient sensitivity of the 1.5T scanner and SWI sequence used in this study in the detection of small white matter susceptibility changes in mild GMH-IVH. Larger studies performed on 3T scanners, using other QSM approaches, are needed to clarify this point. More interestingly, higher susceptibility values in several white matter regions were also detected in the contralateral hemisphere in preterm neonates with unilateral GMH-IVH. Taken together, these findings suggest that large amounts of intraventricular blood may determine an increase of magnetic susceptibility in the normal-appearing white matter surrounding the GMH-IVH, but also in regions distant from the primary site of bleeding. Although no definite explanation could be provided at this time, we speculate that presence of migrating glial cells within the periventricular white matter of infants beyond 20 weeks'

gestation may explain the long-distance migration and accumulation of iron deposits.

Recently, Ley and colleagues revealed extensive amounts of extracellular hemoglobin and its catabolic products in the periventricular white matter of preterm rabbit pups 72 hours after intraventricular hemorrhage. The extracellular hemoglobin released during ongoing hemolysis within the intraventricular space diffused passively through the ependyma driven by concentration gradients, migrating in the white matter in directions of less restricted diffusion. We hypothesize that similar mechanisms may occur also in preterm neonates during the acute phase of GMH-IVH, followed by macrophage-mediated degradation into hemosiderin and ferritin. Ferritin and hemosiderin are the major source of non-heme iron deposition in the human brain, and they induce strong magnetic susceptibility. Although iron is essential for normal brain functioning, iron overload may have devastating effects, inducing a cascade of lipid peroxidation and free radical formation that promote oxidative and inflammatory brain injury lasting for weeks or months after intracranial hemorrhage. In addition, deposition of blood products in distant brain regions may induce diffuse microglial activation, as observed in extreme human preterm brains. Another explanation or contributing factor for this increased magnetic susceptibility may be the secondary white matter microstructural changes observed in preterm neonates with GMH-IVH. Indeed, it has been shown that abnormal brain myelination and consequent white matter microstructure impairment may induce local changes in the magnetic susceptibility, limiting the usual diamagnetic evolution of WM susceptibility during the first period of life. Further studies correlating the QSM results with microstructural analysis obtained with diffusion-weighted imaging are awaited to elucidate how changes in WM microstructure impact on the QSM signal.

This study has several limitations, including its retrospective design and the relatively small number of patients. Moreover, several valid QSM reconstruction algorithms are published, however, we limited the study to the superfast dipole inversion approach because of its simple and straightforward design as compared to other algorithms using nonlinear solvers with data fidelity and weighting terms which impact the quality and quantity of the reconstructed QSM data depending of the chosen regularization parameters. Furthermore, QSM data represents only susceptibility differences and not absolute values. Therefore, QSM values need to be related to a reference region for further comparison. Since CSF and WM are contaminated by residual blood, we limited our study to referencing the susceptibility values to the whole brain. The whole brain, however, includes regions with visible and dispersed blood products in preterm neonates with GMH-IVH and may slightly increase the whole brain susceptibility. Thus, reducing the relative

differences between the magnetic susceptibility differences measured in the normal-appearing white and gray matter especially of patients with severe GMH-IVH compared to controls. However, we still found significantly higher QSM values for the severe GMH-IVH patients. Another limitation is the manual selection of only few representative ROIs, which may render the results prone to subjective errors and does not allow a detailed analysis of the whole brain. On the other hand, manual selection was required in order to avoid visible blood products and infarcted areas. Finally, we relied on the preterm rabbit model for the interpretation of our results, since we did not have the pathological confirmation that the susceptibility differences were in fact related to hemosiderin/ferritin iron secondary to diffusion of extracellular hemoglobin.

In conclusion, paramagnetic susceptibility changes occur in several surrounding and contralateral white matter regions of neonates with severe GMH-IVH compared to controls, likely related to the accumulation of hemosiderin/ferritin iron following diffusion of large amounts of intraventricular blood products into the brain parenchyma. Further studies on larger cohort of preterm neonates using better QSM schemes are needed to confirm these observations.

5.0 CONCLUSIONS

Advanced MRI sequences can assist the standard perinatal brain imaging in the early diagnosis of preterm neonatal brain lesions and can provide new insights for predicting the neurodevelopmental trajectory. However, detailed and serial imaging of carefully chosen cohorts of neonates coupled with longer clinical follow-up are essential to ensure the clinical significance of these new findings.

6.0 FUTURE DEVELOPMENTS

The following investigations are ongoing:

- Correlation analysis between QSM data, DTI data and clinical outcome at 24 months in preterm neonates with GMH-IVH.
- Prospective longitudinal study to evaluate the neurodevelopmental predictive capabilities of brain Functional Connectivity (FC) (evaluated through a multimodal Magnetic Resonance Imaging and Near Infrared Spectroscopy approach) in a large group of preterm neonates studied at term corrected age. This project participated in the call for applied research proposals launched by the Italian Ministry of Health in 2018 (Young Researcher section).

7.0 REFERENCES

1. Chervenak FA. *Fetal and neonatal neurology and neurosurgery*. Churchill Livingstone/Elsevier; 2008.

2. Ramenghi LA, Fumagalli M, Groppo M, et al. Germinal Matrix Hemorrhage: Intraventricular Hemorrhage in Very-Low-Birth-Weight Infants. *Stroke* 2011;42:1889–93.

3. Ramenghi LA, Fumagalli M, Supramaniam V. Brain Development and Perinatal Vulnerability to Cerebral Damage. In: *Neonatology*. Milano: Springer Milan; 2012:1067–78.

4. Rutherford MA, Supramaniam V, Ederies A, et al. Magnetic resonance imaging of white matter diseases of prematurity. *Neuroradiology* 2010;52:505–21.

5. Volpe JJ. Brain injury in premature infants: a complex amalgam of destructive and developmental disturbances. *Lancet Neurol* 2009;8:110–24.

6. Okumura A, Hayakawa F, Kato T, et al. Hypocarbia in preterm infants with periventricular leukomalacia: the relation between hypocarbia and mechanical ventilation. *Pediatrics* 2001;107:469–75.

7. Haynes RL, Folkerth RD, Keefe RJ, et al. Nitrosative and oxidative injury to premyelinating oligodendrocytes in periventricular leukomalacia. *J Neuropathol Exp Neurol* 2003;62:441–50.

8. Deng W, Wang H, Rosenberg PA, et al. Role of metabotropic glutamate receptors in oligodendrocyte excitotoxicity and oxidative stress. *Proc Natl Acad Sci U S A* 2004;101:7751–6.

9. Banker BQ, Larroche JC. Periventricular leukomalacia of infancy. A form of neonatal anoxic encephalopathy. *Arch Neurol* 1962;7:386–410.

10. Volpe JJ. *Neurology of the newborn*. Saunders/Elsevier; 2008.

11. Inder TE, Huppi PS, Warfield S, et al. Periventricular white matter injury in the premature infant is followed by reduced cerebral cortical gray matter volume at term. *Ann Neurol* 1999;46:755–60.

12. Cornette LG, Tanner SF, Ramenghi LA, et al. Magnetic resonance imaging of the infant brain: anatomical characteristics and clinical significance of punctate lesions. *Arch Dis Child Fetal Neonatal Ed* 2002;86:F171-7.

13. Ramenghi LA, Fumagalli M, Righini A, et al. Magnetic resonance imaging assessment of brain maturation in preterm neonates with punctate white matter lesions. *Neuroradiology* 2007;49:161–7.

14. Calloni SF, Cinnante CM, Bassi L, et al. Neurodevelopmental outcome at 36 months in very low birth weight premature infants with MR diffuse excessive high signal intensity (DEHSI) of cerebral white matter. *Radiol Med* 2015;120:1056–63.

15. Pierson CR, Folkerth RD, Billiards SS, et al. Gray matter injury associated with periventricular leukomalacia in the premature infant. *Acta Neuropathol* 2007;114:619–

31.

16. Haynes RL, van Leyen K. 12/15-Lipoxygenase Expression Is Increased in Oligodendrocytes and Microglia of Periventricular Leukomalacia. *Dev Neurosci* 2013;35:140–54.

17. McQuillen PS, Ferriero DM. Selective vulnerability in the developing central nervous system. *Pediatr Neurol* 2004;30:227–35.

18. Logitharajah P, Rutherford MA, Cowan FM. Hypoxic-ischemic encephalopathy in preterm infants: antecedent factors, brain imaging, and outcome. *Pediatr Res* 2009;66:222–9.

19. Jiang ZD, Brosi DM, Wu YY, et al. Relative maturation of peripheral and central regions of the human brainstem from preterm to term and the influence of preterm birth. *Pediatr Res* 2009;65:657–62.

20. Rushe TM, Rifkin L, Stewart AL, et al. Neuropsychological outcome at adolescence of very preterm birth and its relation to brain structure. *Dev Med Child Neurol* 2001;43:226–33.

21. Doyle LW, Casalaz D, Victorian Infant Collaborative Study Group. Outcome at 14 years of extremely low birthweight infants: a regional study. *Arch Dis Child Fetal Neonatal Ed* 2001;85:F159-64.

22. Ment LR, Hirtz D, Hüppi PS. Imaging biomarkers of outcome in the developing preterm brain. *Lancet Neurol* 2009;8:1042–55.

23. Mukerji A, Shah V, Shah PS. Periventricular/Intraventricular Hemorrhage and Neurodevelopmental Outcomes: A Meta-analysis. *Pediatrics* 2015;136:1132–43.

24. Ley D, Romantsik O, Vallius S, et al. High Presence of Extracellular Hemoglobin in the Periventricular White Matter Following Preterm Intraventricular Hemorrhage. *Front Physiol* 2016;7:330.

25. Kidokoro H, Neil JJ, Inder TE. New MR imaging assessment tool to define brain abnormalities in very preterm infants at term. *AJNR Am J Neuroradiol* 2013;34:2208–14.

26. Miller SP, Ferriero DM, Leonard C, et al. Early brain injury in premature newborns detected with magnetic resonance imaging is associated with adverse early neurodevelopmental outcome. *J Pediatr* 2005;147:609–16.

27. Kidokoro H, Neil JJ, Inder TE. New MR imaging assessment tool to define brain abnormalities in very preterm infants at term. *AJNR Am J Neuroradiol* 2013;34:2208–14.

28. Hintz SR, Barnes PD, Bulas D, et al. Neuroimaging and Neurodevelopmental Outcome in Extremely Preterm Infants. *Pediatrics* 2015;135:e32–42.

29. Anderson PJ, Treyvaud K, Neil JJ, et al. Associations of Newborn Brain Magnetic Resonance Imaging with Long-Term Neurodevelopmental Impairments in Very Preterm Children. *J Pediatr* 2017;187:58–65.e1.

30. Woodward LJ, Anderson PJ, Austin NC, et al. Neonatal MRI to predict neurodevelopmental outcomes in preterm infants. *N Engl J Med* 2006;355:685–94.

31. Woodward LJ, Clark CAC, Bora S, et al. Neonatal white matter abnormalities an important predictor of neurocognitive outcome for very preterm children. Baud O, ed. *PLoS One* 2012;7:e51879.

32. Hintz SR, Vohr BR, Bann CM, et al. Preterm Neuroimaging and School-Age Cognitive Outcomes. *Pediatrics* 2018;142:e20174058.

33. Meoded A, Poretti A, Northington FJ, et al. Susceptibility weighted imaging of the neonatal brain. *Clin Radiol* 2012;67:793–801.

34. Zhang Y, Shi J, Wei H, et al. Neonate and infant brain development from birth to 2 years assessed using MRI-based quantitative susceptibility mapping. *Neuroimage* 2019;185:349–60.

35. Mukherjee P, McKinstry RC. Diffusion Tensor Imaging and Tractography of Human Brain Development. *Neuroimaging Clin N Am* 2006;16:19–43.

36. Dudink J, Kerr JL, Paterson K, et al. Connecting the developing preterm brain. *Early Hum Dev* 2008;84:777–82.

37. Pecheva D, Kelly C, Kimpton J, et al. Recent advances in diffusion neuroimaging: applications in the developing preterm brain. *F1000Research* 2018;7:1326.

38. Telischak NA, Detre JA, Zaharchuk G. Arterial spin labeling MRI: Clinical applications in the brain. *J Magn Reson Imaging* 2015;41:1165–80.

39. Alsop DC, Detre JA, Golay X, et al. Recommended implementation of arterial spin-labeled perfusion MRI for clinical applications: A consensus of the ISMRM perfusion study group and the European consortium for ASL in dementia. *Magn Reson Med* 2015;73:102–16.

40. Massaro AN, Bouyssi-Kobar M, Chang T, et al. Brain perfusion in encephalopathic newborns after therapeutic hypothermia. *AJNR Am J Neuroradiol* 2013;34:1649–55.

41. Doria V, Beckmann CF, Arichi T, et al. Emergence of resting state networks in the preterm human brain. *Proc Natl Acad Sci* 2010;107:20015–20.

42. Bullmore E, Sporns O. Complex brain networks: graph theoretical analysis of structural and functional systems. *Nat Rev Neurosci* 2009;10:186–98.

8.0 LIST OF PUBLICATIONS (Period 02.11.2015 – 19.10.2018):

1. Pacetti M, **Tortora D**, Fiaschi P, Consales A, Piatelli G, Ravegnani M, Cama A, Pavanello M.Burr Holes Revascularization in Three Pediatric Cases of Moyamoya Syndrome: Easy Choice or Insidious Trap? Case Series and Review. Asian J Neurosurg. 2018 Jul-Sep.

2. Scala M, Fiaschi P, Capra V, Garrè ML, **Tortora D**, Ravegnani M, Pavanello M. When and why is surgical revascularization indicated for the treatment of moyamoya syndrome in patients with RASopathies? A systematic review of the literature and a single institute experience. Childs Nerv Syst. 2018 Jul

3. Bertamino M, Severino M, Grossi A, Rusmini M, **Tortora D**, Gandolfo C, Pederzoli S, Malattia C, Picco P, Striano P, Ceccherini I, Di Rocco M; Gaslini Pediatric Stroke Group. ABCC6 mutations and early onset stroke: Two cases of a typical Pseudoxanthoma Elasticum. Eur J Paediatr Neurol. 2018 Jul.

4. Godano E, Morana G, Di Iorgi N, Pistorio A, Allegri AEM, Napoli F, Gastaldi R, Calcagno A, Patti G, Gallizia A, Notarnicola S, Giaccardi M, Noli S, Severino M, **Tortora D**, Rossi A, Maghnie M. Role of MRI T2-DRIVE in the assessment of pituitary stalk abnormalities without gadolinium in pituitary diseases. Eur J Endocrinol. 2018 Jun.

5. **Tortora D**, Severino M, Sedlacik J, Toselli B, Malova M, Parodi A, Morana G, Fato MM, Ramenghi LA, Rossi A. Quantitative susceptibility map analysis in preterm neonates with germinal matrix-intraventricular hemorrhage. J Magn Reson Imaging. 2018 May

6. Morana G, Lanteri P, **Tortora D**, Martinetti C, Garaventa A. Spinal nerve roots contrast enhancement following anti-GD2 antibody therapy in neuroblastoma. Neurology. 2018 May

7. **Tortora D**, Severino M, Pacetti M, Morana G, Mancardi MM, Capra V, Cama A, Pavanello M, Rossi A. Noninvasive Assessment of Hemodynamic Stress Distribution after Indirect Revascularization for Pediatric Moyamoya Vasculopathy. AJNR Am J Neuroradiol. 2018 Apr

8. Morana G, **Tortora D**, Staglianò S, Nozza P, Mascelli S, Severino M, Piatelli G, Consales A, Lequin M, Garrè ML, Rossi A. Pediatric astrocytic tumor grading: comparison between arterial spin labeling and dynamic susceptibility contrast MRI perfusion. Neuroradiology. 2018 Apr.

9. Whelan CD, Altmann A, Botía JA, Jahanshad N, Hibar DP, Absil J, Alhusaini S, Alvim MKM, Auvinen P, Bartolini E, Bergo FPG, Bernardes T, Blackmon K, Braga B, Caligiuri ME, Calvo A, Carr SJ, Chen J, Chen S, Cherubini A, David P, Domin M, Foley S, França W, Haaker G, Isaev D, Keller SS, Kotikalapudi R, Kowalczyk MA, Kuzniecky R, Langner S, Lenge M, Leyden KM, Liu M, Loi RQ, Martin P, Mascalchi M, Morita ME, Pariente JC, Rodríguez-Cruces R, Rummel C, Saavalainen T, Semmelroch MK, Severino M, Thomas RH, Tondelli M, **Tortora D**, Vaudano AE, Vivash L, von Podewils F, Wagner J, Weber B, Yao Y, Yasuda CL, Zhang G, Bargalló N, Bender B, Bernasconi N, Bernasconi A, Bernhardt BC, Blümcke I, Carlson C, Cavalleri GL, Cendes F, Concha L, Delanty N, Depondt C, Devinsky O, Doherty CP, Focke NK, Gambardella A, Guerrini R, Hamandi K, Jackson GD, Kälviäinen R, Kochunov P, Kwan P, Labate A, McDonald CR, Meletti S, O'Brien TJ, Ourselin S, Richardson MP, Striano P, Thesen T, Wiest R, Zhang J, Vezzani A, Ryten M, Thompson PM, Sisodiya SM. Structural brain abnormalities in the common epilepsies assessed in a worldwide ENIGMA study. Brain. 2018 Feb

10. Morana G, Alves CA, **Tortora D**, Finlay JL, Severino M, Nozza P, Ravegnani M, Pavanello M, Milanaccio C, Maghnie M, Rossi A, Garrè ML. T2*-based MR imaging (gradient echo or susceptibility-weighted imaging) in midline and off-midline intracranial germ cell tumors: a pilot study. Neuroradiology. 2018 Jan

11. Morana G, Alves CA, **Tortora D**, Severino M, Nozza P, Cama A, Ravegnani M, D'Apolito G, Raso A, Milanaccio C, da Costa Leite C, Garrè ML, Rossi A. Added value of diffusion weighted imaging in pediatric central nervous system embryonal tumors surveillance. Oncotarget. 2017 Oct 25

12. **Tortora D**, Martinetti C, Severino M, Uccella S, Malova M, Parodi A, Brera F, Morana G, Ramenghi LA, Rossi A. The effects of mild germinal matrix-intraventricular haemorrhage on the developmental white matter microstructure of preterm neonates: a DTI study. Eur Radiol. 2017 Sep 27

13. **Tortora D**, Severino M, Accogli A, Martinetti C, Vercellino N, Capra V, Rossi A, Pavanello M Moyamoya vasculopathy in PHACE syndrome: six new cases and review of the literature. World Neurosurg. 2017 Sep 5

14. Toselli B, **Tortora D**, Severino M, Arnulfo G, Canessa A, Morana G, Rossi A, Fato MM. Improvement in White Matter Tract Reconstruction with Constrained Spherical Deconvolution and Track Density Mapping in Low Angular Resolution Data: A Pediatric Study and Literature Review. Front Pediatr. 2017 Aug 2017

15. Morana G, Piccardo A, **Tortora D**, Puntoni M, Severino M, Nozza P, Ravegnani M, Consales A, Mascelli S, Raso A, Cabria M, Verrico A, Milanaccio

C, Rossi A. Grading and outcome prediction of pediatric diffuse astrocytic tumors with diffusion and arterial spin labeling perfusion MRI in comparison with 18F-DOPA PET. Eur J Nucl Med Mol Imaging. 2017 Jul 27

16. Severino M, Righini A, **Tortora D**, Pinelli L, Parazzini C, Morana G, Accorsi P, Capra V, Paladini D, Rossi A. MR Imaging Diagnosis of Diencephalic-Mesencephalic Junction Dysplasia in Fetuses with Developmental Ventriculomegaly. AJNR Am J Neuroradiol. 8 Aug 2017

17. **Tortora D**, Mattei PA, Navarra R, Panara V, Salomone R, Rossi A, Detre JA, Caulo M Prematurity and brain perfusion: Arterial spin labeling MRI. NeuroImage: Clinical 2017 Aug 8

18. **Tortora D**, Severino M, Malova M, Parodi A, Morana G, Sedlacik J, Govaert P, Volpe JJ, Rossi A, Ramenghi LA. Differences in subependymal vein anatomy may predispose preterm infants to GMH-IVH. Arch Dis Child Fetal Neonatal Ed. 2017 2017 May 28

19. Merello E, Tattini L, Magi A, Accogli A, Piatelli G, Pavanello M, **Tortora D**, Cama A, Kibar Z, Capra V, De Marco P. Exome sequencing of two Italian pedigrees with non-isolated Chiari malformation type I reveals candidate genes for cranio-facial development". Eur J Hum Genet. 2017 May 17.

20. Severino M, **Tortora D**, Toselli B, Uccella S, Traverso M, Morana G, Capra V, Veneselli E, Fato MM, Rossi A. Structural Connectivity Analysis in Children with Segmental Callosal Agenesis. AJNR Am J Neuroradiol. 2017 Jan 19.

21. Tassano E, Severino M, Rosina S, Papa R, **Tortora D**, Gimelli G, Cuoco C, Picco P. "Interstitial de novo 18q22.3q23 deletion: clinical, neuroradiological and molecular characterization of a new case and review of the literature". Mol Cytogenet. 2016 Oct 10

22. Sampaio L, Morana G, Severino M, **Tortora D**, Leão M, Rossi A. "Torcular pseudomass: a potential diagnostic pitfall in infants and young children". Pediatr Radiol. 2016 Nov 8.

23. Parodi A, Ramenghi LA, Malova M, **Tortora D**, Severino M, Morana G, Rossi A. "Crossed Pontine Hemiatrophy Associated with Unilateral Cerebellar Hemorrhage in Premature Infants". Neuropediatrics. 2016 Dec;47(6):404-407. PMID: 27552027

24. Severino M, Bertamino M, **Tortora D**, Morana G, Uccella S, Bocciardi R, Ravazzolo R, Rossi A, Di Rocco M. "Novel asymptomatic CNS findings in patients

with ACVR1/ALK2 mutations causing fibrodysplasia ossificans progressiva". J Med Genet. 2016 Dec;53(12):859-864. doi: 10.1136/jmedgenet-2016-104076.

25. Rossi A, Martinetti C, Morana G, Severino M, **Tortora D**. "Neuroimaging of Infectious and Inflammatory Diseases of the Pediatric Cerebellum and Brainstem". Neuroimaging Clin N Am. 2016 Aug;26(3):471-87.

26. Rossi A, Martinetti C, Morana G, Severino M, **Tortora D**. "Diagnostic Approach to Pediatric Spine Disorders". Magn Reson Imaging Clin N Am. 2016 Aug;24(3):621-44. doi:10.1016/j.mric.2016.04.001. Review.

27. **Tortora D**, Severino M, Malova M, Parodi A, Morana G, Ramenghi LA, Rossi A "Variability of cerebral deep venous system in preterm and at term neonates evaluated on MR-SWI venography" AJNR Am J Neuroradiol 2016 Jul 28.

28. Morana G, Puntoni M, Garrè ML, Massollo M, Lopci E, Naseri M, Severino M, **Tortora D**, Rossi A, Piccardo A "Ability of 18F-DOPA PET/CT and fused 18F-DOPA PET/MRI to assess striatal involvement in pediatric gliomas" Eur J Nucl Med Mol Imaging. 2016 Aug;43(9):1664-72.

OTHER ACTIVITIES

Invited speaker to national and international congresses and courses.

1. "Modificazioni del neuroimaging sedazione-dipendenti" 14th Congress Pediatric Section AINR 11-13 October 2018, Brescia Italy

2. "High end objective quantitative MRI" 41st Annual Meeting of The European Society of Neuroradiology 19-23 September 2018, Rotterdam The Nederlands

3. "Advanced MRI in pre-term babies" IX ISMRM Italian Chapter 10-11 May 2018 Padova Italy

4. "Building the connectome". XXI Symposium Neuroradiologicum. 18-23 March 2018 Taipei Taiwan

5. "BOLD signal changes in the neonatal period" IV Congress Functional Section AINR. 3-4 November 2017 Parma Italy

6. " Picking the right outcome measure – Neuroimaging" The II international Conference on Pediatric Anesthesia and Neurotoxicity. 13-14 May 2017 Genoa Italy

7. “MRI and metabolic disorders” MRI of the neonatal brain. 12 January 2017 Utrecht The Netherlands

8. “Perfusion based imaging” MRI of the neonatal brain. 11 January 2017 Utrecht The Netherlands

9. “ fMRI and DTI: specific pediatric issue” Epilepsy Surgery For Focal Cortical Dysplasia 1-2 December 2016 Genoa Italy

10. "Il Prematuro: aspetti neuroradiologici predittivi dell'outcome - SWI" 13th Congress Pediatric Section AINR 7-9 October 2016 Rome Italy

11. “La perfusione senza mezzo di contrasto in pediatria” Course of Brain perfusion imaging 18 March 2016 Rome Italy

Genoa, 08.05.2019

Domenico Tortora